The Astrophysical Journal, 704:324–340, 2009 October 10 doi:10.1088/0004-637X/704/1/324

LESS THAN 10 PERCENT OF STAR FORMATION IN $z \sim 0.6$ MASSIVE GALAXIES IS TRIGGERED BY MAJOR INTERACTIONS

Aday R. Robaina[1], Eric F. Bell[1], Rosalind E. Skelton[1], Daniel H. McIntosh[2,3], Rachel S. Somerville[4], Xianzhong Zheng[5], Hans-Walter Rix[1], David Bacon[6], Michael Balogh[7], Fabio D. Barazza[8], Marco Barden[9], Asmus Böhm[10], John A. R. Caldwell[11], Anna Gallazzi[1], Meghan E. Gray[12], Boris Häussler[12], Catherine Heymans[13], Knud Jahnke[1], Shardha Jogee[14], Eelco van Kampen[9,15], Kyle Lane[12], Klaus Meisenheimer[1], Casey Papovich[16], Chien Y. Peng[17], Sebastián F. Sánchez[18], Ramin Skibba[1], Andy Taylor[19], Lutz Wisotzki[10], and Christian Wolf[20]

[1] Max-Planck-Institut für Astronomie, Königstuhl 17, D-69117 Heidelberg, Germany; arobaina@mpia.de
[2] Department of Astronomy, University of Massachusetts, 710 North Pleasant Street, Amherst, MA 01003, USA
[3] Department of Physics, University of Missouri-Kansas City, Kansas City, MO 64110, USA
[4] Space Telescope Science Institute, 3700 San Martin Dr., Baltimore, MD 21218, USA
[5] Purple Mountain Observatory, Chinese Academy of Sciences, Nanjing 210008, China
[6] Institute of Cosmology and Gravitation, University of Portsmouth, Hampshire Terrace, Portsmouth PO1 2EG, UK
[7] Department of Physics and Astronomy, University of Waterloo, Waterloo, Ontario N2L 3G1, Canada
[8] Laboratoire d'Astrophysique, École Polytechnique Fédérale de Lausanne (EPFL), Observatoire, CH-1290 Sauverny, Switzerland
[9] Institute for Astro- and Particle Physics, University of Innsbruck, Technikerstr. 25/8, A-6020 Innsbruck, Austria
[10] Astrophysikalisches Institut Potsdam, An der Sternwarte 16, D-14482 Potsdam, Germany
[11] University of Texas, McDonald Observatory, Fort Davis, TX 79734, USA
[12] School of Physics and Astronomy, University of Nottingham, Nottingham NG7 2RD, UK
[13] Department of Physics and Astronomy, University of British Columbia, 6224 Agricultural Road, Vancouver V6T 1Z1, Canada
[14] Department of Astronomy, University of Texas at Austin, 1 University Station, C1400 Austin, TX 78712-0259, USA
[15] European Southern Observatory, Karl-Schwarzschild-Str. 2, D-85748 Garching, Germany
[16] Steward Observatory, The University of Arizona, 933 North Cherry Avenue, Tucson, AZ 85721, USA
[17] NRC Herzberg Institute of Astrophysics, 5071 West Saanich Road, Victoria V9E 2E7, Canada
[18] Centro Hispano Aleman de Calar Alto, C/Jesus Durban Remon 2-2, E-04004 Almeria, Spain
[19] The Scottish Universities Physics Alliance (SUPA), Institute for Astronomy, University of Edinburgh, Blackford Hill, Edinburgh EH9 3HJ, UK
[20] Department of Physics, Denys Wilkinson Bldg., University of Oxford, Keble Road, Oxford OX1 3RH, UK
Received 2009 April 20; accepted 2009 August 26; published 2009 September 22

ABSTRACT

Both observations and simulations show that major tidal interactions or mergers between gas-rich galaxies can lead to intense bursts of star formation. Yet, the *average* enhancement in star formation rate (SFR) in major mergers and the contribution of such events to the cosmic SFR are not well estimated. Here we use photometric redshifts, stellar masses, and UV SFRs from COMBO-17, 24 μm SFRs from *Spitzer*, and morphologies from two deep *Hubble Space Telescope* (*HST*) cosmological survey fields (ECDFS/GEMS and A901/STAGES) to study the enhancement in SFR as a function of projected galaxy separation. We apply two-point projected correlation function techniques, which we augment with morphologically selected very close pairs (separation $<2''$) and merger remnants from the *HST* imaging. Our analysis confirms that the most intensely star-forming systems are indeed interacting or merging. Yet, for massive ($M_* \geqslant 10^{10}\,M_\odot$) star-forming galaxies at $0.4 < z < 0.8$, we find that the SFRs of galaxies undergoing a major interaction (mass ratios $\leqslant$1:4 and separations $\leqslant$40 kpc) are only 1.80 ± 0.30 times higher than the SFRs of non-interacting galaxies when averaged over all interactions and all stages of the interaction, in good agreement with other observational works. Our results also agree with hydrodynamical simulations of galaxy interactions, which produce some mergers with large bursts of star formation on $\sim$100 Myr timescales, but only a modest SFR enhancement when averaged over the entire merger timescale. We demonstrate that these results imply that only $\lesssim$10% of star formation at $0.4 \leqslant z \leqslant 0.8$ is *triggered directly* by major mergers and interactions; these events are *not* important factors in the build-up of stellar mass since $z = 1$.

Key words: galaxies: evolution – galaxies: general – galaxies: interactions – galaxies: starburst – galaxies: statistics – infrared: galaxies

Online-only material: color figure

1. INTRODUCTION

Observational evidence from a variety of angles indicates that galaxy interactions and mergers of galaxies can lead to dramatically enhanced star formation (Sanders et al. 1988; Barton et al. 2000, 2007; Lambas et al. 2003). This appears to hold true at all redshifts where one can recognize mergers through galaxy morphologies ($z \lesssim 1$ with rest-frame optical morphologies; Melbourne et al. 2005; Hammer et al. 2005; $1 \lesssim z \lesssim 3$ using less certain UV morphologies; Chapman et al. 2004). Ultraluminous infrared galaxies (ULIRGs), representing the highest-intensity star formation events at low redshifts, are almost invariably hosted by merging galaxies (Sanders et al. 1988). For a number of applications, the quantity of interest is the *average* enhancement in star formation (SF) triggered by merging (ensemble average over the population of major mergers/interactions, or equivalently, temporal average over major merger events during a merger lifetime), not the high-intensity tail (e.g., Barton et al. 2000; Lambas et al. 2003; Hernández-Toledo et al. 2005; Lin et al. 2007; Li et al. 2008; Jogee et al. 2009). Barton et al. (2007) carefully quantified the star formation rate (SFR) enhancement in mergers in low-mass halos at low redshift, using

the Two-Degree Field Galaxy Redshift Survey (Colless et al. 2001). They found that roughly 1/4 of galaxies in close pairs (separated by <50 kpc) in low-mass halos with $M_{b_J} < -19$ have SFR enhancements of a factor of 5 or more.[21]

It has also been noted that the strong decrease of the cosmic SFR density between $z = 1$ and $z = 0$ (e.g., Lilly et al. 1996; Madau et al. 1996; Hopkins 2004; Le Floch et al. 2005) was not dissimilar from the relatively rapid drop in merger rate inferred (at that time) from close pairs and morphologically selected mergers (Le Fèvre et al. 2000). If much of the star formation at $z > 0.5$ were triggered by merging, the apparent similarity in evolution between SFR and merger rate would be a natural consequence. More recently, studies of the fraction of star formation in morphologically selected interacting and merging galaxies at intermediate redshifts $z < 1$ have demonstrated that, in fact, the bulk of star formation is in quiescently star-forming disk-dominated galaxies (Hammer et al. 2005; Wolf et al. 2005; Bell et al. 2005; Jogee et al. 2009).

Similarly, it has long been argued that early-type (elliptical and lenticular) galaxies are a natural outcome of galaxy mergers (e.g., Toomre & Toomre 1972; Schweizer & Seitzer 1992). In any hierarchical cosmogony, mergers are expected to play a large role; a wide range of work—observations of the increasing number density of non-star-forming early-type galaxies from $z = 1$ to the present (Bell et al. 2004; Brown et al. 2007; Faber et al. 2007), the kinematic and stellar populations of local early-type galaxies (Trager et al. 2000; Emsellem et al. 2004), or the joint evolution of the stellar mass function and SFRs of galaxies (Bell et al. 2007; Walcher et al. 2008; Pérez-González et al. 2008)—has given support to the notion that at least some of the early-type galaxies assembled at $z < 1$ have done so through galaxy merging. In such a picture, the average SFR enhancement from merging is of interest for interpreting the SF and chemical enrichment history of early-type galaxies, inasmuch as it gives an idea of what kind of fraction of stars in present-day early-type galaxies we can expect to have formed in the burst mode, and what fraction we can expect to have formed in a quiescent mode in the progenitor galaxies.

Direct observational constraints on the enhancement in SFR caused by merging provide an important calibration for modeling triggered star formation in cosmologically motivated galaxy formation models. Hydrodynamic simulations of interacting galaxies in which gas and star formation are explicitly modeled have demonstrated that torques resulting from the merger can efficiently strip gas of its angular momentum, driving it to high densities and leading to significant enhancement in star formation (e.g., Barnes & Hernquist 1996; Mihos & Hernquist 1996; Cox 2004; Cox et al. 2006a, 2008; di Matteo et al. 2007). However, state-of-the-art cosmological simulations lack the dynamic range to accurately simulate the internal structure of galaxies in significant volumes, so estimates of the global implications of merger-driven star formation enhancement have had to rely on semianalytic calculations (e.g., Somerville et al. 2001; Baugh et al. 2005; Somerville et al. 2008). Furthermore, as the progenitor properties play a key role in the simulated SFR enhancements (e.g., di Matteo et al. 2007; Cox et al. 2008), inaccurate progenitor property values (e.g., incorrect gas fraction or internal structure) will lead to incorrect estimates for the average fraction of SF in mergers even if the SF in each individual merger were modeled perfectly.

Therefore, to constrain galaxy evolution models and to understand the physical processes responsible for the main mode of star formation at $z < 1$, it is of interest to determine observationally the typical enhancement[22] in SFR averaged over the duration of the entire major (stellar-mass ratio between 1:1 and 1:4) galaxy merger or interaction and to constrain the overall fraction of SF triggered by mergers/interactions at intermediate redshift. In a companion paper (Jogee et al. 2009) we focus on the rate of merging and also present a preliminary exploration of the average change in the SFR caused by late-stage major and minor merging (see also Kaviraj et al. 2009), finding an average mild enhancement within the restrictions imposed by the sample size. In this paper, we present a statistically robust analysis of the properties of star-forming galaxies at $0.4 < z < 0.8$ including all relevant merger phases and aimed at providing a satisfactory answer to two key questions. What is the average enhancement in SFR as a function of galaxy pair separation compared to their SFR before the interaction? What fraction of star formation is directly triggered by major mergers and interactions?

There are a number of conceptual and practical challenges in such an experiment. Enhancements in SFR produce both a boost in luminosity, but also increase dust content and extinction. At a minimum, one therefore needs dust-insensitive SFR indicators. In addition, simulations have indicated that SF can be enhanced at almost all phases of an interaction from first passage through to after coalescence (e.g., Barnes & Hernquist 1996; di Matteo et al. 2007); although close pairs will inevitably include some fraction of galaxies before first pass and galaxies with unbound orbits. Therefore, an analysis needs to include both close pairs of galaxies (those before coalescence) and morphologically classified mergers (primarily those near or after coalescence). Morphological classification is not a straightforward art (see Jogee et al. 2009, for a comparison between automated classifications and visual morphologies), even in ideal cases (Lisker 2008). Finally, galaxy mergers are rare and short-lived, necessitating large surveys to yield substantive samples of mergers.

In this work, we address these challenges as far as possible (see also Lin et al. 2007 and Li et al. 2008). We use estimates of redshift and stellar mass from the COMBO-17 survey (Wolf et al. 2003; Borch et al. 2006) to define and characterize the sample. Stellar mass selection should limit the effect of enhanced star formation and dust content on the sample definition. We use SFR indicators that are constructed to be dust extinction insensitive, by combining ultraviolet (UV; direct, unobscured light from young stars) and infrared (IR; thermal emission from heated dust, powered primarily by absorption of UV light from young stars) radiation (Bell et al. 2005). Finally, we study a very well-characterized sample of galaxy pairs at $0.4 < z < 0.8$ using weighted projected two-point correlation functions (Skibba et al. 2006; Li et al. 2008), supplementing them at very small separations $\lesssim$15 kpc with very close pairs or merger remnants morphologically selected from two wide *HST* mosaics, GEMS (Rix et al. 2004) and STAGES (Gray et al. 2009), in an attempt to account for all stages of galaxy interactions.

The plan of this paper is as follows. In Section 2, we discuss the data and the methods used to estimate the stellar masses and the SFRs. In Section 3, we describe the sample selection and the method used for the analysis. In Section 4, we present

[21] This corresponds roughly to a mass cut of $5 \times 10^9\ M_\odot$, assuming a stellar $M/L_{b_J} \sim 1$, appropriate for a star-forming blue galaxy with a Chabrier (2003) stellar IMF.

[22] When we refer to SFR enhancement, we define this as the ratio of SFR in some subsample (e.g., close pairs) to the average SFR of all systems in that mass bin.

our estimates of the enhancement in SFR as a function of projected separation. In Section 5, we compare with previous observations, constrain the fraction of SF triggered by major mergers and interactions at $0.4 < z < 0.8$, and compare with simulations of galaxy merging. Finally, in Section 6, we summarize the main findings of this paper. All the projected distances between the pairs used here are proper distances. We assume $H_0 = 70$ km s^{-1} Mpc^{-1}, $\Omega_{\Lambda 0} = 0.7$, and $\Omega_{\rm m0} = 0.3$.

2. THE DATA

2.1. COMBO-17: Redshifts and Stellar Masses

COMBO-17 has to date fully surveyed and analyzed three fields to deep limits in 5 broad and 12 medium passbands (Extended Chandra Deep Field South (ECDFS), A901/2 and S11; see Wolf et al. 2003 and Borch et al. 2006). Using galaxy, star, and quasar template spectra, objects are classified and redshifts assigned for ∼99% of the objects to a limit of $m_R \sim 23.5$ (Wolf et al. 2004). The photometric redshift errors can be described as

$$\frac{\sigma_z}{1+z} \sim 0.007 \times [1 + 10^{0.8(m_R - 21.6)}]^{1/2}, \quad (1)$$

and rest-frame colors and absolute magnitudes are accurate to ∼0.1 mag (accounting for distance and k-correction uncertainties). The astrometry is accurate to ∼0.″1 and the average seeing is 0.″7. It is worth noting that Equation (1) leads to typical redshift errors of $\sigma_z \simeq 0.01$ for bright ($m_R < 21$) and $\sigma_z \simeq 0.04$ for faint ($21 < m_R < 23.5$) galaxies in the $0.4 < z < 0.8$ interval.

The stellar masses were estimated in COMBO-17 by Borch et al. (2006) using the 17-passband photometry in conjunction with a non-evolving template library derived using the PÉGASEstellar population model (see Fioc & Rocca-Volmerange 1997, 1999) and a Kroupa et al. (1993) initial mass function (IMF). Note that the results assuming a Kroupa (2001) or a Chabrier (2003) IMF yield similar stellar masses to within ∼10%. The reddest templates have smoothly varying exponentially declining star formation episodes, intermediate templates have a contribution from a low-level constant level of star formation, while the bluer templates have a recent burst of star formation superimposed.

The masses are consistent with those using M/L estimates based on a single color (e.g., Bell et al. 2003). Random stellar mass errors are <0.3 dex on a galaxy-by-galaxy basis, and systematic errors in the stellar masses were argued to be at the 0.1 dex level (see Borch et al. 2006, for more details). Bell & de Jong (2001) argued that galaxies with large bursts of recent star formation could produce stellar M/L values at a given color that are lower by up to 0.5 dex; this uncertainty is more relevant in this work than is often the case. While this will inevitably remain an uncertainty here, we note that the Borch et al. (2006) templates do include bursts explicitly, thus compensating for the worst of the uncertainties introduced by bursting star formation histories. In Section 4.1.2, we will explicitly study the impact that such uncertainties have on our results.

In what follows, we use COMBO-17 data for two fields: the ECDFS and Abell 901/902 fields, because of their complementary data: deep *HST*/ACS imaging from the GEMS and STAGES projects, respectively (allowing an investigation of morphologically selected merger remnants and very close pairs), and deep 24 μm imaging from the MIPS instruments on board *Spitzer*, required to measure obscured SF.

2.2. GEMS and STAGES HST Imaging Data

F606W (V-band) imaging from the GEMS and STAGES surveys provides 0.″1 resolution images for our sample of COMBO-17 galaxies. Using the Advanced Camera for Surveys (ACS; Ford et al. 2003) on board the *Hubble Space Telescope* (*HST*), areas of $\sim 30' \times 30'$ in each of the ECDFS and the A901/902 field have been surveyed to a depth allowing galaxy detection to a limiting magnitude of $m^{AB}_{\rm lim}(F606W) = 28.5$ (Rix et al. 2004; Gray et al. 2009; Caldwell et al. 2008). These imaging data are later used to visually classify galaxies, allowing very close pairs (separations <2″) and merger remnants to be included in this analysis. We choose not to use F850LP *HST* data available for the GEMS survey in order to be consistent in our classification between the two fields (only F606W is available from STAGES).

2.3. MIPS 24 μm, Total Infrared Emission and Star Formation Rates

The IR observatory *Spitzer* has surveyed two of the COMBO-17 fields: a $1^\circ \times 0.^\circ 5$ scan of the ECDFS (MIPS GTO), and a similarly sized field around the Abell 901/902 galaxy cluster (MIPS GO-3294: PI Bell). The final images have a pixel scale of 1.″25 pixel^{-1} and an image point spread function (PSF) FWHM of ≃6″. Source detection and photometry are described in depth in Papovich et al. (2004) and catalog matching in Bell et al. (2007).[23] Based on those works, we estimate that our source detection is 80% complete at the 5σ limit of 83 μJy in the 24 μm data in the ECDFS for a total exposure of ∼1400 s pixel^{-1}. The A901/902 field has similar exposure time, but owing to higher (primarily zodiacal) background the 5σ limit (80% completeness) is 97 μJy, with lower completeness of 50% at 83 μJy. We use both catalogs to a limit of 83 μJy.

To include both obscured and unobscured star formation into the estimate of the SFR of galaxies in our sample, we combine UV emission with an estimate of the total IR luminosity in concert. As the total thermal IR flux in the 8–1000 μm range is observationally inaccessible for almost all galaxies in our sample, we have instead estimated total IR luminosity from the observed 24 μm flux, corresponding to rest-frame 13–17 μm emission at the redshifts of interest $z = 0.4$–0.8. For this exercise, we adopt a Sbc template from the Devriendt et al. (1999) SED library (Zheng et al. 2007b; Bell et al. 2007). The resulting IR luminosity is accurate to a factor of $\lesssim$2: local galaxies with IR luminosities in excess of $> 10^{10}\,L_\odot$ show a tight correlation between rest-frame 12–15 μm luminosity and total IR luminosity (Spinoglio et al. 1995; Chary & Elbaz 2001; Roussel et al. 2001; Papovich & Bell 2002) with a scatter of ∼0.15 dex. Furthermore, Zheng et al. (2007b) have stacked luminous ($L_{\rm TIR} \gtrsim 10^{11}\,L_\odot$) $z \sim 0.7$ galaxies at 70 μm and 160 μm, finding that their average spectrum is in good agreement with the Sbc template from Devriendt et al. (1999), validating at least on average our choice of IR SED used for extrapolation of the total IR luminosity.

We estimate the SFR by using both directly observed UV-light from massive stars and dust-obscured UV-light measured from the mid-infrared. As in Bell et al. (2005) we estimate the SFR ψ by means of a calibration derived from PÉGASE synthetic

[23] In this paper, we are interested in SFR enhancements in close pairs of galaxies, where the closest pairs may fall within a single *Spitzer*/MIPS PSF. Accordingly, in this work we choose to explore the total SFR in the pair (avoids deblending uncertainties) rather than the individual SFR occurring in both galaxies.

models assuming a 100 Myr old stellar population with constant SFR and a Chabrier (2003) IMF

$$\psi/(M_\odot\ \mathrm{yr}^{-1}) = 9.8 \times 10^{-11} \times (L_{\mathrm{TIR}} + 2.2 L_{\mathrm{UV}}). \quad (2)$$

Here, L_{TIR} is the total IR luminosity and $L_{\mathrm{UV}} = 1.5 \nu l_{\nu,2800}$ is a rough estimate of the total integrated 1216–3000 Å UV luminosity. This UV luminosity has been derived from the 2800 Å rest-frame luminosity from COMBO-17 $l_{\nu,2800}$. The factor of 1.5 in the 2800 Å-to-total UV conversion accounts for UV spectral shape of a 100 Myr old population with constant SFR, and the UV flux is multiplied by 2.2 to account for the light emitted longwards of 3000 Å and shortwards of 1216 Å by the unobscured stars belonging to the young population.

For all galaxies detected above the 83 μJy limit, we have used the IR and UV to estimate the total SFR. For galaxies undetected at 24 μm, or detected at less than 83 μJy, we use instead UV-only SFR estimates.

2.3.1. IR Emission from AGN-heated Dust

Possible contamination of mid-IR-derived SFRs from active galactic nucleus (AGN)-heated dust is often addressed by estimating the fraction of star formation held in X-ray detected sources. In our case <15% of the star-forming galaxy sample were detected in X-rays, in good agreement with the results found by, i.e., Silva et al. (2004) or Bell et al. (2005).

Yet, there are two limitations of this estimate. First, this does not account for any contribution from X-ray undetected Compton-thick AGN, which could drive up the expected contribution from AGN in our sample. For example, applying an $m_R = 24$ cut to the sample of Alonso-Herrero et al. (2006), we estimate the fraction of X-ray undetected AGN to be ∼30%, while Risaliti et al. (1999) find ∼50% of local AGN to be Compton thick. On this basis, it is conceivable that up to 30% of 24 μm luminosity is from galaxies with AGN.[24]

Second, even in galaxies with AGN, not all of the IR emission will come from the AGN. Although the data do not currently exists to answer this question conclusively, it is possible to make a rough estimate of the effect. In order to estimate the fraction of mid-IR light that comes from the AGN (as opposed to star formation in the host), we have made use of the results of Ramos Almeida et al. (2007), who attempted to structurally decompose mid-infrared imaging from *Infrared Space Observatory* for a sample of both Seyfert 1 and 2 AGN in the local universe, some of which are very highly obscured in X-rays. Analyzing the results in Tables 2 and 3 of Ramos Almeida et al. (2007), we have found that only a small fraction of the IR radiation at ∼10 μm (in this paper we work at rest frame 13–17 μm) comes from the central parts of the galaxies in the Seyfert 2 population, finding a total contribution of

$$\frac{F_{\mathrm{IR}}^{\mathrm{AGN}}}{F_{\mathrm{IR}}^{\mathrm{total}}} = 0.26 \pm 0.02. \quad (3)$$

This result should be viewed as indicative only: obviously, the systems being studied will be different in detail from those in our sample. Furthermore, the 10 μm luminosities of the nuclei will be preferentially affected by silicate absorption, making it possible that our value of $F_{\mathrm{IR}}^{\mathrm{AGN}}/F_{\mathrm{IR}}^{\mathrm{total}}$ is a lower limit.

[24] Although note that in a recent investigation of X-ray undetected IR-bright galaxies in the CDFS, Lehmer et al. (2008) found that radio-derived (1.4 GHz) SFRs agree with the UV+IR-derived ones. This implies that the relative strength of any AGN component is not dominant when compared to the host galaxy.

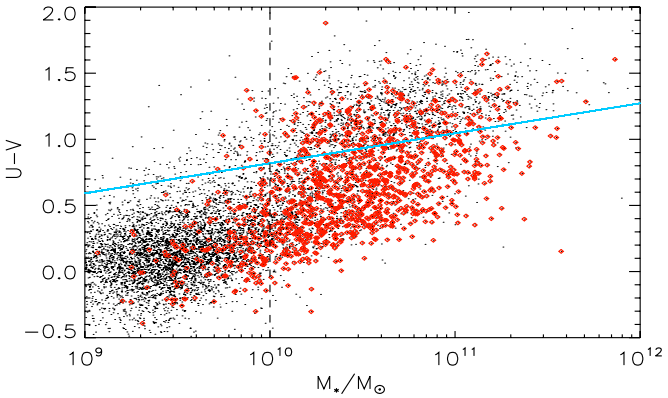

Figure 1. Stellar mass vs. color distribution of COMBO-17 selected galaxies in the ECDFS and A901/2 field with $0.4 < z < 0.8$. The vertical line shows the mass limit $M_\star > 10^{10}\,M_\odot$ used to select our sample. This mass selected sample is complete except for red sequence galaxies at $z > 0.6$. The blue line shows the cut used to separate red sequence and blue cloud galaxies. Red symbols denote 24 μm detected galaxies with >83 μJy.

(A color version of this figure is available in the online journal.)

Despite the various levels of uncertainty, taking the different lines of evidence together demonstrates that $\lesssim$30% of the IR luminosity in our sample comes from systems that may host an AGN, and that it is likely that <10% of the IR luminosity of our sample is powered by accretion onto supermassive black holes. Given the other uncertainties in our analysis, we choose to neglect this source of error in what follows.

3. SAMPLE SELECTION AND METHOD

The goal of this paper is to explore the SFR in major mergers between massive galaxies, from the pre-merger interaction to after the coalescence of the nuclei. We chose a stellar mass-limited sample with $M_\star \geqslant 10^{10}\,M_\odot$ in the redshift slice of $0.4 < z \leqslant 0.8$ (see Figure 1). This roughly corresponds to $M_V = -18.7$ for galaxies in the red sequence and $M_V = -20.1$ for blue objects. We only included galaxies that fall into the footprint of both the ACS surveys GEMS and STAGES and of existing *Spitzer* data. These criteria resulted in a final sample of 2551 galaxies.

Given the flux limit $m_R \lesssim 23.5$ for which COMBO-17 has reasonably complete redshifts (Wolf et al. 2004) we are complete for $M_* > 10^{10}\,M_\odot$ blue cloud galaxies over the entire redshift range $0.4 < z < 0.8$. For red sequence galaxies, the sample becomes somewhat incomplete at $z > 0.6$, and at $z = 0.8$, the limit is closer to $2 \times 10^{10}\,M_\odot$. We chose to adopt a limit of $10^{10}\,M_\odot$ in what follows, despite some mild incompleteness in the red sequence, for two reasons. First, adopting a cut of $2 \times 10^{10}\,M_\odot$ across the whole redshift range reduces the sample size by a factor of 30%, leaving too small a sample for the proposed experiment. Second, the vast majority of the star-forming galaxies are blue cloud galaxies (83% of the star formation is occurring in blue galaxies), making the modest incompleteness in the red sequence of minor importance.

Later, we will use a subsample composed of star-forming galaxies. We will refer to "star formers" as galaxies defined by having either blue optical colors or having been detected in the MIPS 24 μm band. We select optically blue galaxies adopting a stellar mass-dependent cut in rest-frame $U-V$ color, following

Bell et al. (2007; see our Figure 1)[25]:

$$U - V \gtrsim 1.06 - 0.352z + 0.227(\log_{10} M_* - 10).$$

We include all objects detected above the 24 μm limit of 83 μJy as star forming.

In order to track star formation in very close pairs (<2″ and hence unresolved by the ground-based COMBO-17 data) and merger remnants, we include only merging systems (from the ACS data) with $M_* > 2 \times 10^{10}\, M_\odot$: i.e., the minimum possible mass for a merger between two galaxies in our sample.

3.1. Projected Correlation Function

The correlation function formalism is a convenient and powerful tool to characterize populations of galaxy pairs (e.g., Davis & Peebles 1983; Beisbart & Kerscher 2000). Here, we use weighted projected two-point correlation functions because redshift uncertainties (1%–3%) from COMBO-17 translate to line-of-sight distance errors of ∼100 Mpc, necessitating the use of projected correlation functions to explore the properties of close physical pairs of galaxies (Bell et al. 2006). For our sample at hand, we estimate the weighted (or marked) two-point correlation function (Boerner et al. 1989; Beisbart & Kerscher 2000; Skibba et al. 2006; Skibba & Sheth 2009), using both the SFR and the specific SFR (SFR per unit stellar mass) as the weight.

The projected correlation function $w(r_P)$ is the integral along the line of sight of the real-space correlation function

$$w(r_p) = \int_{-\infty}^{\infty} \xi\left(\left[r_p^2 + \pi^2\right]^{1/2}\right) d\pi, \tag{4}$$

where r_p is the distance between the two galaxies projected on the plane of sky and π the line-of-sight separation. A simple estimator for this unweighted correlation function is $w(r_p) = \Delta(DD/RR - 1)$, where Δ is the path length being integrated over, $DD(r_P)$ is the histogram of separations between real galaxies and $RR(r_P)$ is the histogram of separations between galaxies in a randomly distributed catalog (this is the same estimator used in Bell et al. 2006). Basically, the aim is to find the excess probability (compared to a random distribution) of finding a galaxy at a given distance of another galaxy. This estimator accomplishes that by subtracting the random probability of finding two galaxies at a given separation from the probability in the real data sample and normalizing to the probability in the random case. Other estimators (i.e., $\Delta[(DD - DR)/RR]$ or $\Delta[(DD - 2DR + RR)/RR]$) for the two-point correlation function give results different by <5% (less than other sources of uncertainty). Thus,

$$DD(r_P) = \sum_{ij} D_{ij},$$

$$RR(r_P) = \sum_{ij} R_{ij},$$

where the sum is over all non-repeated pairs in the sample, and D_{ij} (R_{ij}) equals 1 only if the pair-selection criteria are satisfied in the real (random) galaxy catalog, and is equal to 0 otherwise.

[25] Due to minor magnitude and color calibration differences between the two fields, the red sequence cut is slightly field dependent, with the intercept at $10^{10}\, M_\odot$ and $z = 0$ being $U - V = 1.01$ and 1.06 for the ECDFS and the A901/902 fields.

The first criterion is that the stellar-mass ratio falls between 1:1 and 1:4. We further only allow a maximum redshift difference $\Delta z = \Delta = \sqrt{2}\sigma_z$, where σ_z is the error in redshift of the primary galaxy (see Equation (1)), and, depending on the case, either the primary or both galaxies in the pair have to be star formers (see Section 4).

We can then study the possible enhancement of (specific) SFR by means of a projected marked (or weighted) correlation function, which can be defined

$$E(r_p) = \frac{1 + W(r_p)/\Delta}{1 + w(r_p)/\Delta}, \tag{5}$$

where $W(r_p) = \Delta(PP/PP_R - 1)$ and

$$PP(r_P) = \sum_{ij} P_{ij} D_{ij},$$

$$PP_R(r_P) = \sum_{ij} P_{ij} R_{ij}.$$

P_{ij} is the mark (or weight). We adopt two different weights P_{ij} in what follows, one is the SFR of the pair of galaxies

$$P_{ij} = S_{ij} = \mathrm{SFR}_{ij} = \mathrm{SFR}_i + \mathrm{SFR}_j,$$

and the other is the specific SFR of the galaxy pair

$$P_{ij} = s_{ij} = \text{Specific SFR}_{ij} = \frac{\mathrm{SFR}_i + \mathrm{SFR}_j}{M_{\star,i} + M_{\star,j}}.$$

Then, the estimator that we use for $E(r_p)$ is

$$E(r_p) = \frac{PP/DD}{\langle P_{ij} \rangle}, \tag{6}$$

where $\langle P_{ij} \rangle$ is the average value of the weight used (SFR, or specific SFR) across the sample. This normalization is the average value of pair SFR or SSFR for the actual pair samples used in this analysis, out to a projected separation of 8 Mpc, in order to probe galaxy pairs sampling different environments to build a representative cosmic-averaged weight. The SFRs or SSFRs of individual galaxies used to find the normalization are exactly the same as for the numerator, as described in Section 2.3. It is worth noting that with our definition of the enhancement given in Equation (5) the random histograms RR and PP_R cancel in the process of obtaining the expression in Equation (6), so they are not used in the computation of our enhancement.

In the present work we perform two analyses: the cross-correlation of star-forming galaxies (as defined above) as primary galaxies with all galaxies as secondaries, and the autocorrelation of star-forming galaxies. We will estimate the errors in our mark by means of bootstrapping resampling.

3.2. Visual Morphologies

A particular challenge encountered when constructing a census of star formation in pairs and mergers is accounting for systems with separations of <2″ (which corresponds to <15 kpc, the radius within which we can no longer separate two massive galaxies using COMBO-17; Bell et al. 2006). In order to pick up the SF in all the stages of the interaction, we need to have an estimate of the SFR not only in galaxy pairs with separations >15 kpc but also in extremely close pairs and in recent merger remnants. We conduct our census of such close

physical pairs by including in the <15 kpc range sources that are not resolved by COMBO-17, but appear to be interacting pairs or merger remnants on the basis of visual classification of the ∼0.″1 resolution ACS images. We try to recover visually all <15 kpc separation pairs of two $M_* > 10^{10}\,M_\odot$ galaxies with a mass ratio between 1:1 and 1:4 missed by COMBO-17. In addition to those extremely close pairs, we also account for the SF in recent merger remnants $M_* > 2 \times 10^{10}\,M_\odot$ (two times the minimum mass of a galaxy in the sample and the minimum possible mass of a galaxy pair as defined before).

3.2.1. Discussion of Visual Classifications

Our goal is to include very close pairs or already-coalesced major merger remnants into the census of "mergers" in order to account for any SF triggered by the merger/interaction process.[26] We do so on the basis of visual classification of the sample. The motivation for visual classification is a pragmatic one: while a number of automated morphological classification systems have been developed in the last 15 years (i.e., Abraham et al. 1996; Conselice et al. 2003; Lotz et al. 2004, etc.), it seems that the sensitivity of the observables used (asymmetry, clumpiness, Gini coefficient, second-order moment of the 20% brightest pixels) is insufficient for matching the performance of visual classification in current intermediate redshift galaxies with the same level of precision that they display in the local universe samples used for their calibration (Conselice et al. 2003; Lisker 2008; Jogee et al. 2009).

Yet, there is a degree of subjectivity to what one deems to be a major merger remnant. Many factors shape the morphology of a galaxy merger that are beyond the control of the classifier. Bulge-to-total (B/T) mass ratios have an strong effect on both the intensity of the SFR enhancement and the time at which the intensity peak shall occur (e.g., Mihos & Hernquist 1996). Orbital parameters strongly shape the development of easily recognizable tidal tails and bridges (coplanar or not, retrograde versus prograde, etc.). Prior dust and gas content of the parent galaxies ("dry" versus "wet" mergers) will make a difference to the appearance of the final object during the coalescence. Furthermore, merging timescales will depend on whether the galaxies are undergoing a first passage or are in the final stages of the merger. Finally, there is a degeneracy between all these parameters and the relative masses of the galaxies undergoing the interaction, which makes difficult in some cases to distinguish the morphological signatures of a major merger from those of a minor merger.

Some of these factors (e.g., gas fraction, B/T ratios, etc.) will also affect the enhancement of the SFR during the interaction (e.g., di Matteo et al. 2007, 2008; Cox et al. 2008). While there is considerable merger-to-merger scatter, encounters of two gas-rich disk galaxies with parallel spins tend to develop, on average, the strongest morphological features, but at the same time are more likely to throw out large amounts of cold gas in tidal tails, preventing the funneling of this gas to the central regions. Thus, samples selected to have the strongest morphological features may have an average SFR enhancement different from the actual mean enhancement.[27]

One practical issue is that of passband choice and shifting. We choose to classify the F606W images of the GEMS and STAGES fields (in STAGES because that is the only available *HST* passband and in GEMS for consistency and because F606W has higher S/N that the F850LP data). This corresponds to rest-frame ∼430(330)*nm* at redshift 0.4(0.8). In previous papers (Wolf et al. 2005; Bell et al. 2005; Jogee et al. 2009), we have assessed whether the morphological census derived from GEMS/STAGES would change significantly if carried out data a factor of 5 deeper from the GOODS project (testing sensitivity to surface brightness limits), or if carried out at F850LP (always rest-frame optical at these redshifts). We found that the population does not show significantly different morphologies between our (comparatively) shallow F606W data and the deeper/redder imaging data from GOODS (see Figure 5 in Jogee et al. 2009).

3.2.2. Method

An independent visual inspection of the galaxy sample has been carried out by four classifiers, A.R.R., E.F.B., R.E.S., and D.H.M., in order to identify morphological signatures of major gravitational interactions. Each classifier assigned every one of the ∼2500 sample members to one of the three following groups.

1. Non-major interactions: the bulk of galaxies in this bin show no signatures of gravitational interactions. Asymmetric, irregular galaxies with patchy star formation triggered by internal processes lie in this category. A small fraction of galaxies in this bin show a clearly recognizable morphology (e.g., spiral structure) but also signatures of an interaction (such as tidal tails, or warped, thick or lopsided disks) but have no clear interaction companion; note that these objects could be interacting systems where the companion is now reasonably distant and/or faint and more difficult to identify. The tidal enhancement of SF from such systems will *not* be missed by putting them in this bin; rather, it will be measured statistically and robustly from the two point correlation function analysis. Minor mergers and interactions (interactions where the secondary is believed, on the basis of luminosity ratio, to be less than 1/4 of the mass of the primary) also belong to this category.
2. Major close interactions: close pairs resolved in *HST* imaging but not in ground-based COMBO-17 data, consisting of two galaxies with mass ratios between 1:1 and 1:4 based on relative luminosity, and clear signatures of tidal interaction such as tidal tails, bridges or common envelope (see Figure 2). From now on we shall refer to objects classified in this group as "very close pairs."
3. Major merger remnants: objects that are believed to be the coalesced product of a recent major merger between two individual galaxies. Signposts of major merger remnants include a highly disturbed "train wreck" morphology, double nuclei of similar luminosity, tidal tails of similar length, or spheroidal remnants with large-scale tidal debris (see Figure 3). Galaxies with clear signs of past merging but a prominent disk (e.g., highly asymmetric spiral arms or one tidal tail) were deemed to be minor merger remnants and were assigned into the Group 1. Naturally, there is some uncertainty and subjectivity in the assignment of this class, in particular; such uncertainty is taken into account in our analysis by the Monte Carlo sampling of all four classifications in order to properly estimate the dispersion in the opinions of the individual classifiers (see below).

[26] Note that a consistent comparison with the projected correlation function sample requires the inclusion of all non-interacting pairs that are physically associated (in the same cluster, filament, etc.), are seen to be close projected pairs on the sky, but may be separated by as much as a few Mpc along the line of sight.

[27] This bias might also be present in the case of studies looking for signs of interactions in the host galaxies of AGNs, attempting to assess whether the AGN activity is preceded by a merger.

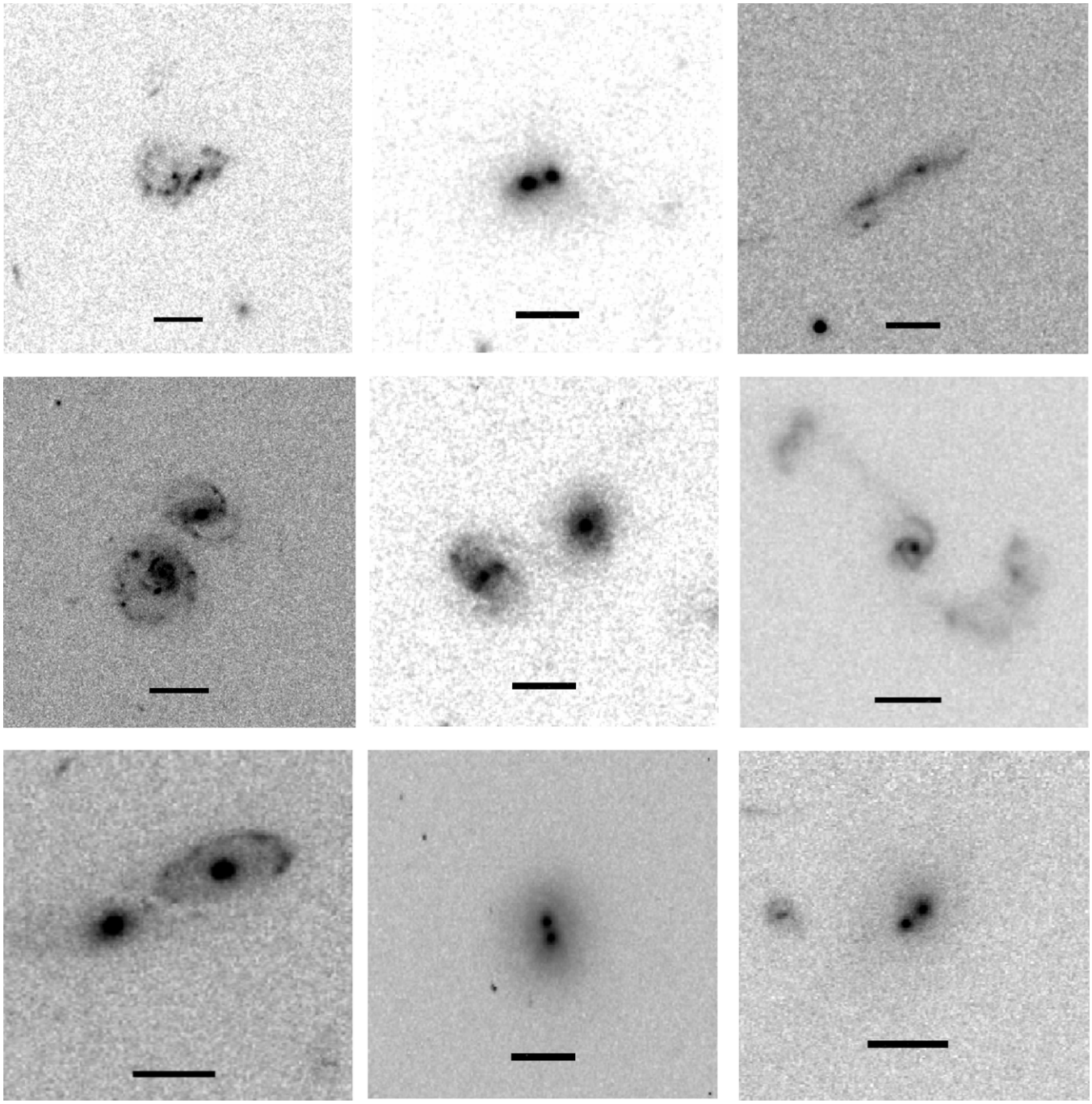

Figure 2. Objects classified in Group 2: major close interactions. The presence of two galaxies and signs of interaction are required. The classifier believes the mass ratio is between 1:1 and 1:4. At this stage of the interaction, dry mergers are still recognizable as seen in panels at top center, bottom center and bottom right. The black bar at the bottom of every panel shows a proper distance of 20 kpc at the redshift of the object. Some of the objects classified in this group were also separated as two galaxies in the ground-based catalog and treated in consequence.

We then assign the objects in the Groups 2 and 3 (very close pairs with morphological signatures of interaction and merger remnants, respectively) to a small projected separation and treat every one of them as a galaxy pair in order to combine them with the correlation function analysis result for pairs with separations $>2''$. All objects in Group 2 (extremely close pairs with projected separations <15 kpc as measured by centroids in *HST* imaging) are assigned to a separation of 10 kpc and all objects in Group 3 (merger remnants) are assigned to a separation of 0 kpc. We have checked for duplicate pairs in both the visually selected sample and the COMBO-17 catalog in order to avoid repeated pairs. Galaxies in Group 1 are already included in the two point correlation function analysis, and any SF triggered by major interactions or early-stage major merging is accounted for by that method. As we have four different classifications for every object (one given by each human classifier), we randomly assign one of them, calculate the average value of the weight we are using and repeat the process a number of times. As by definition objects in Groups 2 and 3 are considered to be a galaxy pair by themselves, we remove in every Monte Carlo realization the objects assigned to those groups before we run the weighted correlation function. This approach presents two clear advantages: (1) the resultant bootstrapping error not only represents the statistical dispersion

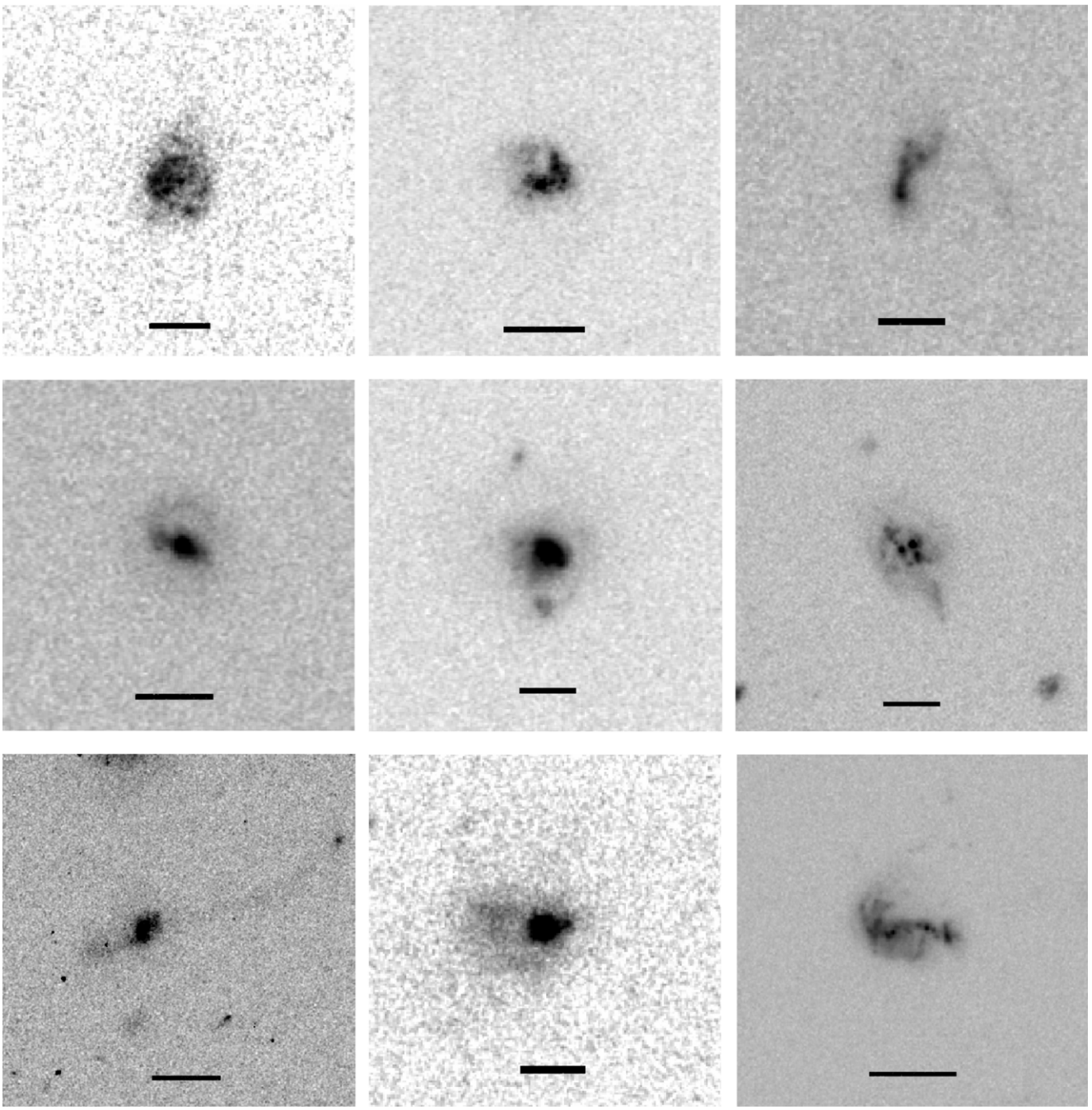

Figure 3. Objects classified in Group 3: major merger remnants. The black bar at the bottom of every panel shows a proper distance of 20 kpc at the redshift of the object.

but also the different criteria of the four human classifiers; and (2) the morphology of every object is weighted with *the four* classifications given. This means that objects with discrepant classifications are not just assigned to one category when we calculate the SFR (or specific SFR) enhancement; rather, any dispersion in classifications is naturally accounted for (e.g., minor/major criteria). The numbers of such systems and their uncertainties, estimated from the classifier-to-classifier scatter, are given in Table 1.

4. RESULTS

We are now in a position to quantify the triggering of star formation in galaxy interactions and mergers in the redshift interval $0.4 < z < 0.8$, in the cases where each galaxy has $M_* > 10^{10}\,M_\odot$ and the pair has a stellar-mass ratio between 1:1 and 1:4. Our primary analysis is based on a marked cross-correlation between star-forming galaxies, as defined in Section 3, and all galaxies in the sample. For morphologically selected very close pairs or interactions (unresolved by COMBO-17), we also require them to be blue or detected by *Spitzer* to be considered as part of the star-forming sample,[28] with a mass of $M_* > 2 \times 10^{10}\,M_\odot$.

We perform two analyses in this paper: the cross-correlation of star formers as primary galaxies with all galaxies as secondaries (our default case), and the autocorrelation of star-forming

[28] All galaxies, irrespective of their color or IR flux, were classified; the star-forming galaxies are simply a subsample of this larger sample.

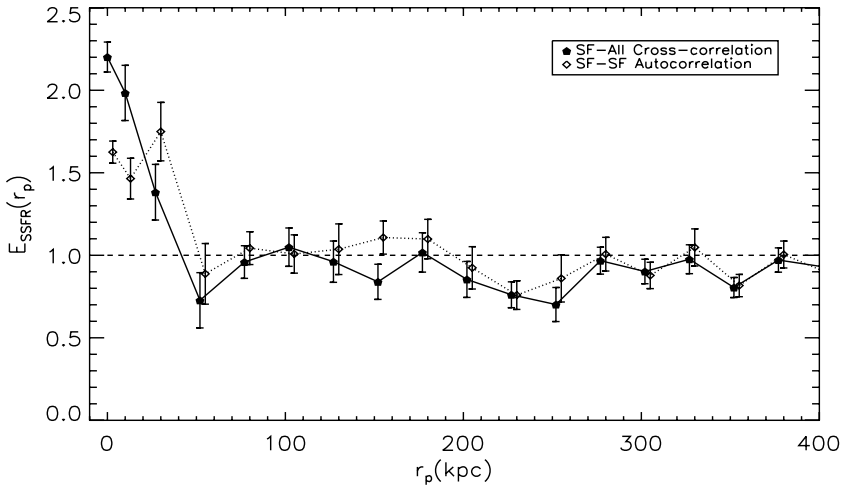

Figure 4. Pair specific SFR enhancement as function of the projected separation between two galaxies. The two smallest radii bins are derived from morphologically selected very close pairs (shown with $r_P \sim 10$ kpc) and merger remnants (shown with $r_P = 0$); enhancements at larger radii are determined using weighted two-point correlation functions. A statistically significant enhancement is present in galaxy pairs and mergers below 40 kpc in both the cross–correlation between star-forming galaxies as primaries and all galaxies as secondaries (black filled symbols) and the autocorrelation of star–forming galaxies (empty diamonds). Error bars have been calculated by bootstrapping.

Table 1
Results from the Morphological Classification

Lower Mass Limit	Sample Size	Group 1	Group 2	Group 3
$10^{10}\ M_\odot$	2551	$2380 \pm 37 \pm 49$	$106 \pm 7 \pm 10$	$72 \pm 7 \pm 8$
$2 \times 10^{10}\ M_\odot$	1749	$1640 \pm 32 \pm 40$	$69 \pm 6 \pm 8$	$44 \pm 5 \pm 7$

Notes. Galaxy and interaction sample. Group 1: isolated objects and minor interactions. Group 2: extremely close pairs ($r_P < 15$ kpc). Group 3: merger remnants. The first error bar represents classifier-to-classifier scatter, while the second one represents Poisson noise.

galaxies. While the first analysis is a rather more direct attack on the question of interest, we show results from the autocorrelation of star-forming galaxies to illustrate the effects of making different sample choices on the final results.

4.1. Enhancement in the Star Formation Activity

Our main results are shown in Figure 4, which shows the enhancement of the specific star formation rate (SSFR) in pairs as a function of their projected separation. As explained in Section 2.3 we use UV+IR SFRs for the objects detected in 24 μm and only UV SFRs for those undetected. For the whole sample, 38% of the galaxies where detected by *Spitzer* above the 83 μm limit, while if we restrict to the Groups 2 and 3 in our morphological classification we find a detected fraction of 60%. Figure 4 shows a clear enhancement in the SSFR for projected pair separations $r_P < 40$ kpc. It could be argued that the SSFR is a better measure of the SF enhancement than the SFR-weighted estimator, because the strong scaling of SFR with galaxy mass is factored out. The figure shows both the cross-correlation between star-forming primaries and all secondaries (SF–All, solid line) and the star-forming galaxy autocorrelation (SF–SF, dotted line). The two bins at $r_p \leqslant 15$ kpc are calculated from morphologically selected very close pairs ($r_p = 10$ kpc) and merger remnants ($r_P = 0$). All the errors in $E_{\rm SSFR}$ have been computed by bootstrap resampling. This approach allows us to treat both the morphologically selected objects and the galaxy pairs exactly in the same way, having as a result a coherent display of the error bars.

There are two reasons why this excess in $E_{\rm SSFR}$ in close pairs and remnants is likely a sign that interactions induce additional star formation, rather than being due to a correlation with some other unidentified quantity: (1) it is well known from simulations (Mihos & Hernquist 1996; di Matteo et al. 2007; Cox et al. 2008) that a burst of star formation is expected in the collisions of gas-rich galaxies; and (2) the observed effect is in the opposite sense of the usual SFR–density relation (e.g., Balogh et al. 2002), which says that galaxies in dense environments (where preferentially close galaxy pairs tend to be found, as shown in Barton et al. 2007) have, on average, weaker star formation activity than galaxies in less dense regions.

Even when we consider our morphological classification and further Monte Carlo resampling method to be very robust, potential classification errors could act in two different directions. Interacting systems misidentified as non-interacting will be diluted into the background star formation as single galaxies contributing to pairs at random separations. While this SF should be lost to the interacting bin, the effect on the average SFR would be minimal. On the other hand, isolated galaxies misidentified as interacting systems because of internal instabilities or stochastic star formation would act to reduce the enhancement.

As mentioned before, the SFR for the objects undetected at 24 μm has been calculated based only on the UV. In the 24 μm detected objects, we have found no clear trend in both the UV versus UV+TIR SFRs and in the TIR/TUV versus optical dust attenuation but found instead a constant correction factor with a large scatter (4.1 ± 2.4 as estimated from the relation between TIR/TUV versus optical attenuation.) We have checked the effects of such a dust-correction of the UV-only SFRs: the results differ in all bins by <10%, comparable to or smaller than other sources of systematic uncertainty.

Yet, in order to understand the degree of obscuration in galaxy interactions we have repeated our analysis including *only* UV–derived SFRs, this is, excluding the TIR component in Equation (2) for 24 μm detections. The result of this analysis is shown in Figure 5. The enhancement in the unobscured SSFR measured for close pairs ($r_P < 40$ kpc) in this case is dramatically smaller than the enhancement including the dust-obscured (IR-derived) SFR. This is more apparent in the very close pairs and merger remnants, where the excess in the SSFR even disappears completely in the case of the SF–SF autocorrelation ($E(r_P < 15\ \text{kpc}) \simeq 1$). This implies that

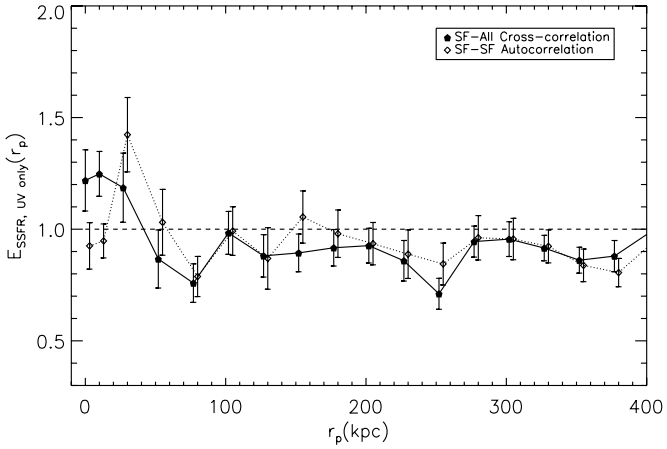

Figure 5. Same as Figure 4 but tracing only unobscured (UV-derived) star formation. The unobscured SSFR enhancement found in galaxy pairs with separations $r_P < 40$ kpc and mergers remnants is dramatically reduced with respect to the case in which the obscured star formation is taken into account (Figure 4).

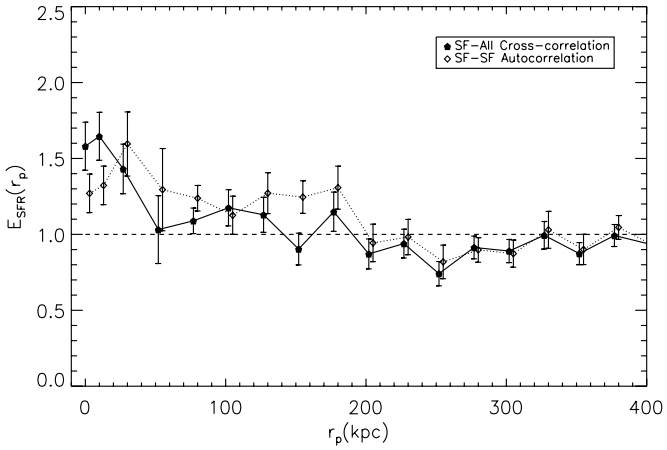

Figure 6. SFR enhancement in galaxy interactions. The two smallest radii bins are derived from morphologically selected extremely close pairs ($r_P \sim 10$ kpc) and merger remnants (shown with $r_P = 0$); enhancements at larger radii are determined using weighted two-point correlation functions. There is a clear enhancement at $r_P < 40$ kpc for the cross-correlation analysis (black-filled symbols) which is compatible with E_{SSFR} (Figure 4) except for the merger remnants, where the excess is ∼50% lower. The autocorrelation of star-forming galaxies (empty symbols) presents an unexpected behavior, showing a very mild enhancement at $r_P < 180$ kpc.

most of the directly triggered star formation is dust obscured, in good agreement with the expectations from Mihos & Hernquist (1994, 1996), di Matteo et al. (2007), Cox et al. (2008), and the detailed models by Jonsson et al. (2006). In these simulations most of the star formation is triggered in the central regions of the galaxy after the cold gas has been funneled to the inner kpc.

This scenario is also supported by our measurement of the mean ratio between the total SFR and the UV-derived, which gives an idea of the degree of dust-obscuration (SFR_{IR+UV}/SFR_{UV}). We find 6.64 ± 0.66 in the case of the merger remnants (Group 3 in Section 3.2) and 6.63 ± 0.64 in the case of the very close pairs (Group 2), compared to 3.15 ± 0.53 for all objects in the sample.

4.1.1. Star Formation Rate versus Specific Star Formation Rate

To study the fraction of the global star formation *directly triggered* by galaxy–galaxy interactions the enhancement in the SFR (rather than in the SSFR) is a better quantity to consider.

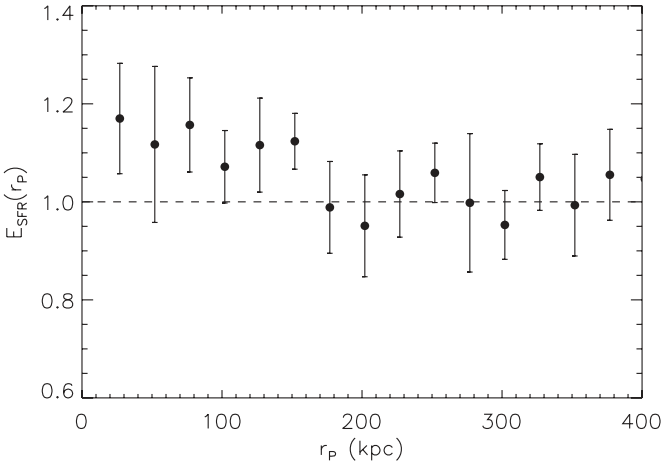

Figure 7. SFR enhancement measured after randomizing the SFR between galaxies of similar stellar mass. A mild enhancement is found out to separations of ∼160 kpc. We show the points corresponding to the SF–SF autocorrelation at distances >15 kpc, where no morphological information is used.

We show in Figure 6 the enhancement in the SFR ($E_{SFR}(r_p)$) as a function of the projected pair separation. For the cross–correlation function (our default case) the enhancement in the SFR is similar to the one found in the SSFR at all separations except for the merger remnants ($r_p = 0$), in which the excess above the whole population is ∼50% lower. The SFR–weighted autocorrelation of star-forming galaxies matches that of the SSFR–weighted one for $r_p < 40$ kpc but differs beyond: $E_{SFR} = 1.25$ for $40 < r_P < 180$ kpc. While most of these points in Figure 6 are individually compatible with the error bars shown in Figure 4, taken together they represent a $\sim 2\sigma$ significant difference between E_{SSFR} and E_{SFR} for the entire region $40 < r_p < 180$ kpc.

A potential driver of the SFR enhancement in the regime $40 < r_P < 180$ kpc is the fact that more massive galaxies tend to be both more clustered and have higher SFR (Noeske et al. 2007); this could translate into a weak enhancement in the SFR in galaxy pairs living in dense environments (see Barton et al. 2007, for a thorough discussion on the relation between galaxy pairs and environment) which will not be present in the SSFR, because the normalization by galaxy mass factors out this dependence. To test the relevance of this systematic effect, we randomized the SFRs among galaxies of similar mass 500 times in the sample and repeated the analysis. We show the results of this exercise in Figure 7, where we can see a tail of enhancement with a behavior similar to the one seen in Figure 6. We believe that a combination of the density–mass–SFR relation plus noise is driving $E_{SFR} > 1$ (autocorrelation) between 40 and 180 kpc.

Accordingly, we consider only the enhancement at $r_P < 40$ kpc as produced by major merging in what follows, and use the differences between the SFR and SSFR enhancement on <40 kpc scales as a measure of systematic uncertainty. Under those assumptions, we find a weak enhancement of star formation at $r_P < 40$ kpc of $\epsilon = 1.50 \pm 0.25$ in the SF–SF autocorrelation and $\epsilon = 1.80 \pm 0.30$ in the SF–All cross-correlation. These values have been computed as the average of the enhancement in the bins $r_P < 40$ kpc *together* in E_{SSFR} and E_{SFR}. These (conservative) error bars include both the statistical uncertainties and the systematics driving the differences between the SFR and the SSFR.

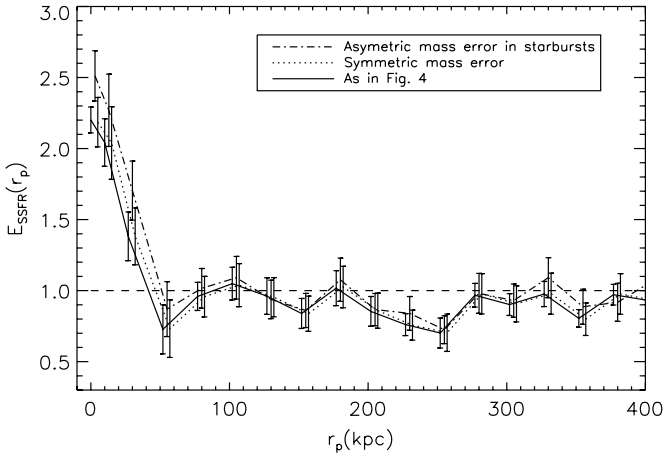

Figure 8. Enhancement in the SSFR including estimates for the errors in the stellar masses. Dotted line: Gaussian error with $\sigma = 0.1$ dex. Dash-dotted line: non-star-forming galaxies with Gaussian error with $\sigma = 0.1$ dex and starburst galaxies (SFR $> 16\,M_{\odot}$ yr^{-1}) with errors following an inverted lognormal distribution to produce a tail to the lower masses, with a shift of 0.1 dex also to the lower masses and $\sigma = 0.2$ dex. Solid line: enhancement in the SSFR as in Figure 4, for comparison.

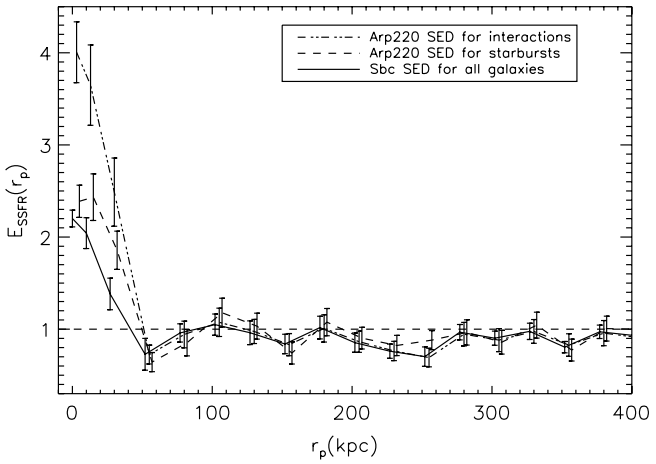

Figure 9. Impact on the SSFR enhancement when using an Arp220 template in the conversion between observed 24 μm and TIR luminosity for certain objects. Red line: extreme case in which we apply an Arp220 template to all interacting systems (and Sbc template to everything else). Green line: Arp220 template applied to objects with SFR $> 16\,M_{\odot}$ yr^{-1} (and Sbc template to everything else). Black line: Same as in Figure 4, for comparison. Red and green lines include the asymmetric stellar mass errors applied in Figure 8.

4.1.2. Further Uncertainties

As we have briefly mentioned in Section 2, there are some uncertainties which need to be estimated in the process of calculating the enhancement in the SF activity. Here we try to estimate the impact of the stellar-mass and IR SED selection uncertainties. Through this section we will focus in our default case, the SF–All cross-correlation.

Random errors in stellar masses in Borch et al. (2006) are <0.1 dex (with 0.3 dex in cases with large starbursts (Bell & de Jong 2001)) on a galaxy-by-galaxy basis, and systematic errors not related to the choice of an universally applied stellar IMF are 0.1 dex. In addition, M/L ratios in starbursting galaxies can be biased to produce unrealistic high stellar masses(Bell & de Jong 2001). Those effects would have certain impact in the calculation of the SSFR, and thus, in the enhancement of that quantity. In order to estimate how those mass uncertainties affect our results, we have run two additional Monte Carlo shufflings. In Figure 8 we show the result of this exercise. We have randomly added a Gaussian error with $\sigma = 0.1$ dex to the stellar masses of all galaxies and repeated the process 500 times, finding an average output value similar to the one presented in Figure 4 but with larger errors. The impact of the new errors on the average enhancement (taking into account also the enhancement in the SFR, as we did in the previous section) is negligible.

In order to estimate the uncertainties introduced by systematics in the M/L ratio of starbursts, we have performed a similar exercise but using an error which includes a systematic shift down of 0.1 dex, $\sigma = 0.2$ dex and a tail to the lower masses defined by an inverted lognormal distribution. We have applied this new error to objects with SFR $> 16\,M_{\odot}$ yr^{-1}, which roughly corresponds to twice the average SFR in our sample of *star-forming* galaxies, and the symmetric error described above to galaxies with SFR $< 16\,M_{\odot}$ yr^{-1}. The result (dash-dotted in Figure 8) shows some extra enhancement in this case, which leads to an average enhancement in the SF activity $\epsilon = 1.85 \pm 0.35$, barely changing the result already found.

Another potential source of uncertainty is the stellar masses of pairs of galaxies not resolved in the ground-based photometry catalog (i.e., our very close pairs group). In order to test the impact of this underdeblending on the galaxy masses, we take U and V rest-frame fluxes of galaxies widely separated, add them together and check what stellar mass would result in the case of applying the Borch et al. (2006) method to a galaxy with exactly the same color as the combination of the two galaxies, and compare with the sum of the two original masses. We find that for pairs of galaxies of all kinds (All–All, SF–SF, and SF–All) there is a <0.01 dex offset and 0.08 dex scatter between the two sets of masses. That is, masses from combined luminosities are the same as the sum of the individual masses to 0.08 dex, what means that our stellar masses are extremely robust against underdeblending issues.

Together with the stellar-masses, the main source of uncertainty in our analysis is the conversion between observed 24 μm and TIR in the process of obtaining the SFRs. Zheng et al. (2007b) have demonstrated that the Sbc template used here is an appropriate choice for this data set at all IR luminosities, but in order to find an absolute upper limit for the final results we will show in Section 5.2 we estimate the different results we would obtain if considering an Arp 220 template in some cases.

We find that at a given 24 μm flux, the use of an Arp 220 template gives a TIR luminosity which is higher than that derived using a Sbc template by a factor of 2. We apply this factor of 2 correction to the TIR luminosity of all the galaxies that we define as starburst for this purpose (SFR $> 16\,M_{\odot}$ yr^{-1}) and show the result as the green line in Figure 9. The enhancement found in this case is $\epsilon = 2.1 \pm 0.4$, consistent with, by higher than the $\epsilon = 1.8 \pm 0.3$ found in Section 4.1.1.

We also want to test the extreme case in which the IR SED of all galaxies undergoing an interaction follows an Arp220 SED, independently of their level of SFR. This is clearly an unrealistic case as we know that some of our galaxies in close pairs and remnants have SFRs as low as 4–5 $M_{\odot}$ yr^{-1} (factor of 10 less SFR than Arp220), and we know also that the average IR SED of $z \sim 0.6$ galaxies with SFRs $\geqslant 10\,M_{\odot}$ yr^{-1} is similar to the Sbc template adopted here (Zheng et al. 2007a), but it is useful in the sense that it provides a strong upper limit beyond the uncertainties of our data and method. The result found in this case can be seen as the red line in Figure 9. Clearly, a much stronger enhancement is present as a consequence of this

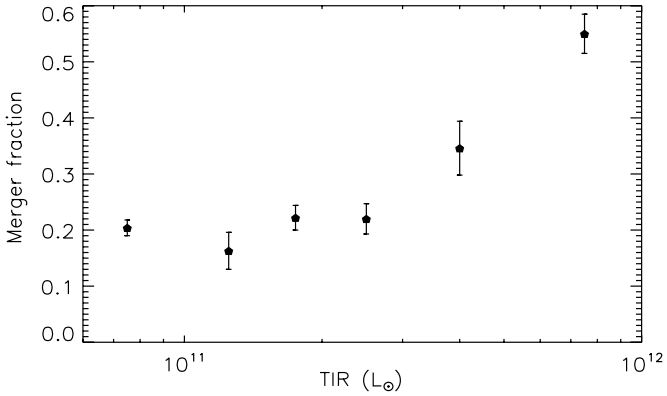

Figure 10. Fraction of systems in close projected pairs $r_p < 40$ kpc or in visually identified mergers as function of the total IR luminosity of all 24 μm detected galaxies in the sample. The merger fraction is ∼20% from our luminosity limit of $6 \times 10^{10}\ L_\odot$ to $3 \times 10^{11}\ L_\odot$. Higher than this luminosity, the merger fraction begins to grow to 55% just below $10^{12}\ L_\odot$.

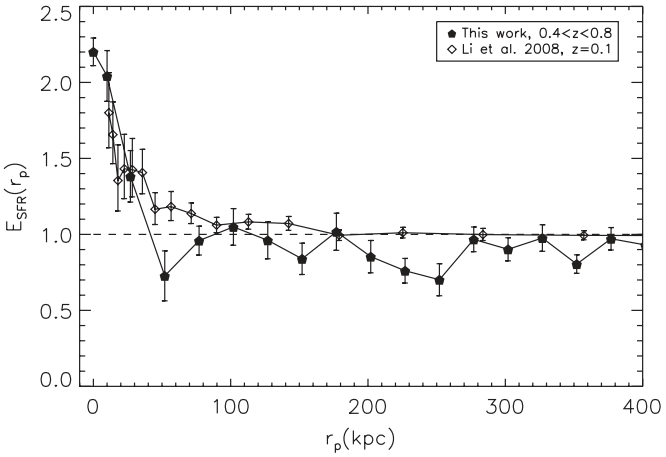

Figure 11. Comparison between the enhancement found in this work (black filled points) and the one found in Li et al. (2008) at $z \simeq 0.1$ (open diamonds). In both cases, a cross-correlation SF–All is shown. Both works show a statistically significant enhancement of the SSFR at $r_P < 40$ kpc.

overestimation of the TIR luminosity, that leads, when taken together with the SFR enhancement calculated in the same way, to $\epsilon = 3.1 \pm 0.6$.

4.2. How Important are Mergers in Triggering Dust-obscured Starbursts?

We have demonstrated that when averaged over all events and all event phases there is a relatively modest SFR enhancement from major galaxy merging and interactions. It is of interest to constrain how the distribution of SFRs differs between the non-interacting and interacting galaxies. Here we present a preliminary result on one aspect of the issue, namely the fraction of infrared-luminous galaxies that are in close pairs $r_p < 40$ kpc or were visually classified as merging systems.

In Figure 10, we show how the fraction of galaxies that are either in close pairs ($r_p < 40$ kpc) or in morphologically classified merger remnants varies as a function of their total IR luminosity. This fraction is constant (∼20%) for $6 \times 10^{10}\ L_\odot < L_{\rm TIR} < 3 \times 10^{11}\ L_\odot$. At higher luminosities, the merger fraction increases as a function of the IR luminosity, reaching 55% just below $L_{\rm TIR} = 10^{12}\ L_\odot$. The lower IR limit of $6 \times 10^{10}\ L_\odot$ was chosen to ensure a flux of 83 μJy over the entire redshift range. The increase in merger fraction at high IR luminosity is in accord with previous results at both low and intermediate redshift (e.g., Sanders et al. 1988). This suggests that merging and interactions are an important trigger of intense, dust-obscured star formation. Apparently, high IR luminosities are difficult to reach without an interaction.

A key point, however, is that *not all* mergers have high IR luminosity. While mergers can produce enormous SFRs, and also $L_{\rm TIR} > 10^{12}\ L_\odot$ is best reached by merging, the typical SFR enhancement in mergers is modest.

5. DISCUSSION

We have assembled a unique data set for galaxies at $0.4 < z < 0.8$ that combines redshifts, stellar masses, SFRs, and *HST* morphologies to explore the role of major mergers and interactions in boosting the SFR. In practice, we have combined projected correlation-function and morphological techniques to estimate the average enhancement of star formation in star-forming galaxies with $M_* > 10^{10}\ M_\odot$ and $0.4 < z < 0.8$, where the average is taken over most merging phases and all mergers. We find an SF enhancement by a modest factor of ∼1.8 for separations of <40 kpc in both the SFR and the SSFR. How does this compare with previous observations and models? What implications does this mild enhancement have on the contribution of major mergers to the cosmic SF history?

5.1. Comparison with Previous Observations

Our analysis is most directly comparable to estimates of SFR enhancement in galaxy close pairs by Li et al. (2008) using the Sloan Digital Sky Survey at $z \sim 0.1$ because of the similarities between our methods. Using a cross-correlation between star-forming and all galaxies, they found an enhancement of $\simeq$1.45 for an average galaxy mass of $\langle \log(M_*/M_\odot) \rangle = 10.6$ within a radius of 15 to ∼35–40 kpc. In Figure 11, we show the comparison between their present-epoch measurements and ours (average galaxy mass $\sim 10^{10.5}\ M_\odot$, SF–All cross-correlation) revealing reasonable quantitative agreement. Both the projected separation scale ($\lesssim 40$ kpc) and the overall amplitude at small projections (×1.5–2) agree. The enhancement found here also agrees (given the error bars) with the enhancement found at $0.75 < z < 1.1$ in Lin et al. (2007). Our results are similar to those at both $z = 0.1$ and at $z = 1$, despite the factors of several difference between the typical SFRs of galaxies between $z = 1$ and $z = 0$ (see, e.g., Zheng et al. 2007a). This is interesting, and points to a picture in which at least the average enhancement of star formation in galaxy interactions appears to be independent of the "pre-existing" star formation in the population.

Lin et al. (2007) also measured an enhancement in the TIR emission in galaxy pairs and mergers in the $0.4 < z < 0.75$ range. They find that the infrared luminosity of close pairs with both members selected to be blue is 1.8 ± 0.4 times that of control pairs, similar to our value 1.75 ± 0.18 for close pairs in the bin 15 kpc $< r_P <$ 40 kpc from the SF–SF autocorrelation. For late-phase mergers, they measure 2.1 ± 0.4, marginally consistent with our 1.54 ± 0.08 from the SF–SF autocorrelation at $r_P = 0$ kpc. Slight differences in that number may be attributed to differences in the "merger" classification. For example, many of the remnants that we include in this study may not be detected by automated methods based on the intensity-weighted Gini-M_{20} or asymmetry parameters. As shown in recent work (Jogee et al. 2009; Miller et al. 2008), automated methods based on CAS asymmetry parameters tend to capture only a fraction (typically 50% to 70%) of the visually identified

merger remnants and often pick up a dominant number of non-interacting galaxies that have small-scale asymmetries associated with dust and star formation.

In a related work (Jogee et al. 2009), we recently estimated the overall merging rate and also addressed the SFR enhancement at $0.24 < z < 0.8$. For the subsample of systems with $M_* > 2.5 \times 10^{10}\,M_\odot$, we find that the average SFR of late stage mergers with mass ratio between 1:1 and 1:10 (both major and minor mergers) are only enhanced by a modest factor (1.5–2 from their Figure 15) with respect to non-interacting galaxies. There are three differences that make it difficult to perform an exact comparison between our works. (1) In the present study we try to isolate the contribution from major interactions (mass ratio 1:1 to 1:4), while in Jogee et al. (2009) we focused on both major and minor interactions (mass ratio from 1:1 to 1:10). (2) The normalization is slightly different because in the present work we compare the SFR in mergers with the SFR in the pair of progenitors, while in Jogee et al. (2009) we compare with the SFR of individual galaxies with mass similar to the interacting system. As the average SFR is a function of the galaxy stellar mass, $2 \times \mathrm{SFR}_{M>10^{10},\mathrm{progenitor}} \neq \mathrm{SFR}_{M>2\times10^{10},\mathrm{descendant}}$. (3) In the present paper we attempt to target both early and late phases of the interaction, while in Jogee et al. (2009) we focus on the later phase. Nonetheless, it is encouraging that the two studies agree qualitatively in finding a modest enhancement in the average SFR in galaxy interactions.

Taken together, we argue that our results are consistent with those of previous works. We have used a bigger sample of galaxies with both *HST*/ACS and *Spitzer*/MIPS coverage than previous works at $z \geqslant 0.4$ and we tried to trace the SFR enhancement in all the stages of the interaction with a consistent treatment of ground-based selected galaxy pairs and morphologically selected pairs and remnants. We view it as extremely encouraging that where the works are the most robust (close pairs), the results are highly consistent (comparing our work with Li et al. 2008 and the pairs from Lin et al. 2007). It is clear that robustly assessing the star formation enhancement in advanced-stage mergers, identifiable using only high-resolution data and morphological techniques, is considerably more challenging. The results for advanced-stage mergers are therefore less well constrained, but are nonetheless all consistent with a modest but significant enhancement in SFR.

5.2. What Fraction of Star Formation is Triggered by Major Interactions?

We can now combine our estimates for the SFR enhancement, the fraction of galaxies in projected close pairs, the average SFR, and the amount of SFR in recognizable merger remnants to quantify what fraction of star formation at $0.4 < z < 0.8$ is *directly triggered* by major interactions. We will not include systematics such as the uncertainty in conversion of 24 μm to total IR, or the effect of the 24 μm flux limit, but we will consider the systematics driving the difference between the SSFR enhancement and the SFR enhancement. We make the cross-correlation between star-forming galaxies as primaries and all galaxies as secondaries our default case because it includes the residual SFR in red galaxies and also traces the SF enhancement in disk galaxies during the encounter with a non-star-forming galaxy. We will also show the values obtained for the SF–SF autocorrelation. We use the values 1.80 ± 0.30 and 1.50 ± 0.25 found in Section 4.1.1 in $r_P <$ 40 kpc systems, for the cross-correlation and the autocorrelation, respectively.

The fraction of galaxies in close physical pairs within a separation r_f can be derived using the following approximation (Patton et al. 2000; Masjedi et al. 2006; Bell et al. 2006):

$$P(r < r_f) = \frac{4\pi n}{3-\gamma} r_0^{\gamma} r_f^{3-\gamma}. \quad (7)$$

Here $P(r < r_f)$ is the fraction of galaxies in the parent sample in pairs with real separations of $r < r_f$, n is the number density of galaxies satisfying the pair-selection criteria, and r_0 and γ are the parameters of the power-law real-space correlation function of the parent sample, subjected to the pair-selection criteria (i.e., we use a stellar-mass ratio of 1:1 to 1:4 as a requirement for a pair to enter into the correlation function).

Note that because in this paper we typically impose criteria for matching and forming pairs (e.g., a mass ratio between 1:1 and 4:1), the number density n used is not the number density of the larger parent sample n_{parent}. The number of possible pairs at any projected separation range is lower than in the case in which no mass ratio criteria is imposed because many pairs with mass ratios beyond the allowed limit are automatically rejected. As the fraction of galaxies in close physical pairs is directly related to the number density of galaxies n, this parameter has to be fine-tuned in order to get the right fraction. The number density used in Equation (7) has to be corrected for the effect that the mass ratio criteria introduces on the total number of potential pairs. Then, the number density of the larger parent sample n_{parent} is not used here, instead we use $n = n_{\mathrm{parent}} N_{\mathrm{pairs}}/[0.5 N_{\mathrm{parent}}(N_{\mathrm{parent}} - 1)]$, where N_{pairs} is the number of pairs that can be formed in the parent sample given the matching criteria, and N_{parent} is the number of galaxies in the parent sample ($N(N-1)/2$ is the expression for the number of possible pairs in the case of simply pairing up the parent sample).

We tested this approximation using the semianalytic galaxy catalog of De Lucia et al. (2006), derived from the Millennium N-body simulation. At $z \sim 0.6$ these simulations matched well the stellar mass function and correlation function of $M_* > 10^{10}\,M_\odot$ galaxies. We find that at $r < 50$ kpc Equation (7) is a good approximation to the actual fraction of galaxies in close pairs in the simulation; at larger separation Equation (7) is increasingly incorrect (this is the subject of a paper in preparation).

From fits to the projected two-point cross-correlation function of our sample, we determine $r_0 = 1.8 \pm 0.2$ Mpc, $\gamma = 2.2 \pm 0.1$ for the real-space correlation function, and $n = 0.0152$ galaxies per cubic Mpc[29]; the latter gives a sample of $N_{\mathrm{gal}} = nV = 1913$ galaxies in the volume probed by this study. This yields $P(r < 40\ \mathrm{kpc}) = 0.06 \pm 0.01$ (i.e., 6% of sample galaxies are in close pairs with real-space separations <40 kpc). With this real-space two-point correlation function, 75% ± 10% of all projected close pairs should be real close physical pairs[30] (Equation (6) of Bell et al. (2006) and confirmed using the Millennium Simulation at the redshift of interest). Thus the fraction of objects in projected close pairs will be $f_{\mathrm{pair,proj}} = 0.06/0.75 = 0.08 \pm 0.02$. This fraction includes projections due to real structures like clusters or filaments, but not the purely random projections due to redshift uncertainties which would be present if we would just count the galaxies in projected close pairs in our catalog.

[29] The correlation function is calculated in proper coordinates, because the process of interest is galaxy merging and close pairs of galaxies have completely decoupled from the Hubble flow.

[30] This is only valid after removing the effect introduced by purely random projections with the correlation function method.

When considering *all pairs* at all separations in our sample with $M_* > 10^{10}\,M_\odot$, mass ratios between 1 : 1 and 1 : 4, and primary galaxies with 24 μm fluxes > 83 μJy and/or blue, the average SFR is $\langle \mathrm{SFR}\rangle_{\mathrm{typical,pair}} = 13.2 \pm 0.6\,M_\odot\ \mathrm{yr}^{-1}$. The *total* SFR in the $N_{\mathrm{rem}} = 38 \pm 5$ recognizable merger remnants is $\mathrm{SFR}_{\mathrm{remnants}} = 753 \pm 97\,M_\odot\ \mathrm{yr}^{-1}$. Thus, we can calculate the fraction of SFR occurring in pairs with separations <40 kpc

$$\frac{N_{\mathrm{gal}} f_{\mathrm{pair,proj}} 0.5\epsilon\ \langle \mathrm{SFR}\rangle_{\mathrm{typical,pair}} + \mathrm{SFR}_{\mathrm{remnants}}}{N_{\mathrm{gal}} 0.5\ \langle \mathrm{SFR}\rangle_{\mathrm{typical,pair}}} = 20\% \pm 3\% \tag{8}$$

for the SF–All correlation. A similar analysis with the SF–SF correlation yields 16% ± 3%. What we have done in the numerator of Equation (8) is to take the typical SFR in our pairs and divide by two in order to get the typical SFR of a galaxy contributing to such pairs. This number is different from the typical SFR in our galaxy sample for two reasons: first, we have imposed a mass–ratio criterion (only allow pairs with mass ratios between 1:1 and 1:4), which makes the averaged SFR in all pairs to be slightly biased high respect random pairs without any mass ratio criterion, and second, the fact that we force the primary galaxy to be a star former (in the case of the cross-correlation) has a similar effect. Then we have multiplied it by the enhancement ϵ in order to take into account the excess SFR triggered by major interactions and introduced the factor N_{gal} to account for all the SFR occurring in those galaxies. A key piece of Equation (8) is the different treatment of merger remnants. The correlation function can tell us what is the fraction with separations between $r_P = 40$ kpc and $r_P = 0$ kpc but we have defined merger remnants as objects which have *already* coalesced, so if we think in terms of the duration of the interaction instead of the separation between the galaxies, these objects would be *beyond* the reach of the correlation function, and have to be treated separately. In the denominator we have only divided by the total SFR occurring in *all* the galaxies contributing to any pair we can form with the already mentioned criteria. The difference between this factor and the total SFR calculated simply adding up the SFR of all galaxies in the sample is 5% and is a consequence of the few galaxies which are not paired with any other galaxy in the sample.

Yet, the fraction of the total SFR that occurs in pairs and remnants with <40 kpc separation does not immediately characterize the SFR *triggered* by interactions, because ∼12% of SF should happen at $r_P < 40$ kpc anyway, as we show below. Only the *excess* star formation in pairs and remnants should be attributed to triggering by interactions:

$$\begin{aligned}&\{(N_{\mathrm{gal}} f_{\mathrm{pair,proj}} 0.5(\epsilon - 1)\langle \mathrm{SFR}\rangle_{\mathrm{typical,pair}}\\ &+ (\mathrm{SFR}_{\mathrm{remnants}} - N_{\mathrm{rem}}\langle \mathrm{SFR}\rangle_{\mathrm{typical,pair}}))/(N_{\mathrm{gal}} 0.5\langle \mathrm{SFR}\rangle_{\mathrm{typical,pair}})\}\\ &= 8\% \pm 3\%.\end{aligned} \tag{9}$$

Again, a similar analysis for the SF–SF autocorrelation yields 5% ± 3%. These values for the excess are 12% lower than those in Equation (8) due to the total number of interacting systems, which is higher than the 8% of galaxies in close pairs mentioned before because it includes the merger remnants that are not taken into account by the correlation function method.

Taking all this together, this analysis shows that only ∼8% of the star formation at $0.4 < z < 0.8$ is triggered by major mergers/interactions. This may seem in disagreement with previous results from "morphological" studies. We therefore compare our results with those of Bell et al. (2005) and Wolf et al. (2005), who found that ∼30% of the global SFR at $z = 0.7$ is taking place in morphologically perturbed systems and with Jogee et al. (2009), where we find a similar result at $0.24 < z < 0.8$.

Both Bell et al. (2005) and Wolf et al. (2005) performed a study of the total SFR occurring in visually classified interacting galaxies in a thin redshift slice $0.65 < z < 0.75$ without imposing a lower mass limit (only an apparent magnitude limit). That is the key difference between those earlier works and ours. We impose a mass cut in this paper of $10^{10}\,M_\odot$ and $2 \times 10^{10}\,M_\odot$ for galaxies and visually classified interactions, respectively. For example, the fraction of SFR in galaxies with $M_* > 1$–$2 \times 10^{10}\,M_\odot$ that Bell et al. (2005) and Wolf et al. (2005) identified as interacting/peculiar is 15%–21%, compared to 20% in Equation (8). Only 1/6 of the star formation in the interacting/peculiar galaxies from Bell et al. (2005) and Wolf et al. (2005) occurs in what we would designate as merger remnants, with the other 5/6 occurring in galaxy pairs. Jogee et al. (2009) argued that 30% of star formation was in systems that they classified as major or minor interactions, with mass limits different from those used in this paper. This value is an upper limit to the fraction of star formation in major mergers where each galaxy has mass $>10^{10}\,M_\odot$, both because of the effect of mass limits, and because minor mergers host much of the star formation in systems that they classified to be interacting. Accounting for these differences, our result is in qualitative agreement with theirs.

However, the key difference is that neither Bell et al. (2005), Wolf et al. (2005) nor Jogee et al. (2009) try to quantify the *excess* of SF in interacting systems, as we do in going from Equation (8) to Equation (9). In summary, our new results here pose no inconsistency with earlier studies, but refine them by quantifying the physically more relevant quantity of SF excess.

We have presented the average enhancement in SFR caused by major mergers of galaxies with masses above $10^{10}\,M_\odot$ at $0.4 < z < 0.8$, deriving that approximately 8% of the SF in the volume is *directly* triggered by major merging. As we have mentioned before, the SFR enhancement ϵ seems to be roughly independent of the quiescent SFR ground level present in the galaxy population, that is, insensitive to the drop in the SFR density of the universe since $z = 1$. If this is true, it means that the fraction of star formation directly triggered by galaxy interactions (given a mass cut) would depend only on the number of galaxies undergoing interactions. Using the evolution of pair fraction found in Kartaltepe et al. (2007) we can infer a directly triggered SF fraction of 1%–2% in the local universe, as well as a fraction of 14%–18% at $z = 1$. On the other hand, assuming no evolution in the pair fraction would keep the merger–triggered fraction at 8% between $z = 0$ and $z = 1$. These numbers have to be taken extremely carefully by the reader, as we present here only a crude extrapolation of our results to different redshifts in order to get an idea of the importance of the merger-driven star formation in the universe.

There are a number of limitations of our result that should be borne in mind. First, we can only include SFRs $\gtrsim 5\,M_\odot\ \mathrm{yr}^{-1}$ for $z \sim 0.6$ galaxies. Therefore, our estimates of the SF contribution from merging may be an upper limit because the merger-driven boost in SFR will cause more objects to satisfy this criterion. Second, there are uncertainties in the conversion of 24 μm to total IR, which could influence the excess star formation in close pairs or mergers by ∼30% (Papovich & Bell 2002; Zheng et al. 2007b); this could be addressed once longer-wavelength, deep *Herschel* PACS observations become available. We can

only calculate an absolute upper limit by using the value of the enhancement found in the extreme case in which the 24 μm to TIR conversion in all the interactions, independently of their luminosity, is calculated using an Arp220 template. Using as input $\epsilon = 3.1 \pm 0.6$ for Equation (9) we would find a directly triggered fraction of 19% $\pm$ 5%, consistent with an scenario in which the underlying level of SF is basically negligible and most of the new stars are being formed in the burst mode. Third, it is conceivable that some enhanced star formation occurs in very late-stage merger remnants that were no longer recognized as remnants and hence were not included in this census. This is both a practical (classification) and conceptual issue: when does one declare a merger remnant a normal galaxy again? Nonetheless, despite these points, the analysis presented here has made it very clear that only a small fraction of star formation in galaxies with $M_* > 10^{10}\,M_\odot$ at $0.4 < z < 0.8$ is triggered by major interactions/mergers.

5.3. Comparison with Theoretical Expectations

Star formation enhancement in mergers has been studied extensively with hydrodynamical *N*-body simulations (e.g., Barnes & Hernquist 1991; Mihos & Hernquist 1994, 1996; Springel 2000; Cox et al. 2006a, 2008; di Matteo et al. 2007). However, large-scale cosmological simulations lack the dynamic range to resolve the internal dynamics of galaxies, crucial for modeling the gas inflows and the associated enhancement in star formation. Therefore, the majority of these studies (except Tissera et al. 2002) have been of binary galaxy mergers with idealized initial conditions, typically bulgeless or late-type disks. In most studies, the properties of these progenitor disks are chosen to be representative of present-day, relatively massive spiral galaxies such as the Milky Way. These studies have shown that the burst efficiency in mergers is sensitive to parameters such as merger mass ratio and orbit, and progenitor gas fraction and bulge content. Therefore, any attempt to use these results in an ensemble comparison must somehow convolve these dependencies with a redshift dependent, cosmologically motivated distribution function for these quantities. In addition, Cox et al. (2006a) have shown that star formation enhancement in mergers can also depend on the treatment of supernova feedback in the simulations. Furthermore, the detailed star formation history during the course of a merger, particularly in the late stages, may depend on the presence of an accreting supermassive black hole (di Matteo et al. 2005).

Let us consider the results from representative examples of such binary merger simulations, by Cox et al. (2008), who studied a broad range of merger mass ratios, gas fractions, and progenitor B/T ratios, as well as exploring the effects of two different SN feedback recipes. The 1:1 merger of two "Milky Way"-like progenitors (shown in their Figure 12) shows an average factor of $\sim$1.5 enhancement in SF over about 2.5 Gyr, and a larger enhancement of a factor of 2–10 for a shorter period of about 0.6 Gyr. The overall average enhancement over the whole merger is about a factor of 2.5, depending on the precise timescale one averages over. Very large enhancements ($\sim$5–10) occur over a very short timescale, $\lesssim$100 Myr. This particular simulation represents the largest expected SF enhancement, as the burst efficiency increases strongly toward equal merger mass ratio. For mergers with 1:2.3 mass ratio (Figure 10 of Cox et al. 2008), there is an enhancement of a factor of $\sim$1.5 for 2.5–3 Gyr, and of 2.5 for about 0.6 Gyr. It is also interesting to note that the SFR in the late stages of the merger, when the galaxy still appears morphologically disturbed (see Figure 7 of Cox et al. 2008) is *depressed* with respect to the isolated case. A diverse set of progenitor morphologies, ranging from ellipticals to late-type spirals, was studied by di Matteo et al. (2007). Overall, their results are qualitatively similar to those from Cox et al. (2008).

The simulations discussed so far aimed to reflect progenitor disks with gas fractions, sizes, and morphologies typical of relatively massive, low-redshift late-type spirals such as the Milky Way: gas fraction $f_g \sim 0.2$; $B/T \sim 0.2$; scale length $r_d \sim 3$ kpc. However, Hopkins et al. (2009) show that the burst efficiency is strong function of progenitor gas fraction, in the sense that higher gas fraction progenitors have *weaker* fractional enhancements. The burst efficiency is a factor of 8 lower for a gas fraction of 90% than for the canonically used value of 20%. It is worth noting here that we find the same level of SF enhancement in major mergers at $z \sim 0.6$ and $z \sim 0.1$, where the gas fractions of the two samples are expected to be rather different (see Section 5.1). Whether or not this is quantitatively at odds with the expectations of Hopkins et al. (2009) remains to be seen. On the other hand, recent results from di Matteo et al. (2008) show no difference between the strength or duration of tidally triggered bursts of star formation in local universe and their higher redshifts counterparts, in good agreement with the present study.

To place results in a cosmological context, Somerville et al. (2008) used the results from a large suite of hydrodynamic merger simulations (Cox et al. 2006b, 2006c; Robertson et al. 2006a, 2006b, 2006c) to parameterize the dependence of burst efficiency and timescale on merger mass ratio, gas fraction, progenitor circular velocity, redshift, and the assumed effective equation of state. They implemented these scalings within a cosmological semianalytic merger tree model. We applied our selection criteria to mock catalogs from Somerville et al. (2008), by comparing the fraction of SFR produced in the triggered mode in galaxies with $M_* > 2 \times 10^{10}\,M_\odot$ in our redshift range which suffered a major merger in the last 500 Myr with the total SFR occurring in galaxies $M_* > 10^{10}\,M_\odot$. We found that approximately 7% of the SFR in the volume is produced in the burst mode triggered by major mergers. This is in excellent agreement with the 8% $\pm$ 3% of the overall SFR being directly triggered by major interactions we showed in the previous section.

6. CONCLUSIONS

To quantify the *average* effect of major mergers on SFRs in galaxies, we have studied the enhancement of SF caused by major mergers between galaxies with $M_* > 10^{10}\,M_\odot$ at $0.4 < z < 0.8$. We combined redshifts and stellar masses from COMBO-17 with high-resolution imaging based on *HST*/ACS data for two fields (ECDFS/GEMS and A901/STAGES) and with SFRs that draw on UV and deep 24 μm data from *Spitzer* to form a sample a factor of 2 larger than previous studies in this redshift range. We then applied robust two-point correlation function techniques, supplemented by morphologically classified very close pairs and merger remnants to identify interacting galaxies. Our main findings are as follows.

1. Major mergers and interactions between star-forming massive galaxies trigger, on average, a mild enhancement in the SFR in pairs separated by projected distances $r_P \lesssim 40$ kpc; we find an enhancement of $\epsilon = 1.80 \pm 0.30$ considering the SF–All cross-correlation, where only one galaxy in the pair is required to be forming stars. For a similar analysis

using the autocorrelation of star-forming galaxies we find $\epsilon = 1.50 \pm 0.25$.

2. Our results agree well with previous studies of SF enhancement using close pairs at $z < 1$. In particular, the behavior of SF enhancement at $z = 0.1$, $z = 0.6$, and $z = 1$ appear to be rather similar, indicating that the average SFR enhancement in galaxy interactions is independent of the "pre-existing" SFR in the population.
3. We combine our estimate of the average SFR enhancements in major mergers with the global SFR to show that overall, $8\% \pm 3\%$ of the total star formation at these epochs is *directly* triggered by major interactions. We conclude that major mergers are an insignificant factor in stellar mass growth at $z < 1$.
4. Major interactions do, however, play a key role in triggering the most intense dust-obscured starbursts: we find that the majority of galaxies with IR-luminosities in excess of $3 \times 10^{11}\ L_{\odot}$ are visually classified as ongoing mergers or found in projected pairs within <40 kpc separation. This is not in disagreement with the small *average* SFR enhancement if the most intense SF bursts last only ∼100 Myr.
5. Our results for the SF enhancement appear to be in qualitative agreement with the extensive suite of hydrodynamical simulations by di Matteo et al. (2007, 2008) and Cox et al. (2008), who produce both intense, short-lived bursts of SF in some interactions, but yet produce average enhancements of only 25%–50% averaged over the ∼2 Gyr timescale taken to complete the merger. Furthermore, we find excellent agreement between the fraction of the total SFR directly triggered by major merging measured here and the 7% calculated from mock catalogs obtained from Somerville et al. (2008).

We thank the anonymous referee for the thorough report and many comments which greatly improved this paper. We thank Cheng Li for sharing with us his results in the electronic form. A.R.R. thanks Alejo Martínez-Sansigre and Arjen van der Wel for productive discussions which helped to improve this paper. A.R.R. and E.F.B. gratefully acknowledge support through the Deutsche Forschungsgemeinschaft's Emmy Noether Programme. B.H. acknowledges support by STFC. A.R.R. also acknowledges the Heidelberg-International Max Planck Research School program.

REFERENCES

Abraham, R. G., et al. 1996, MNRAS, 279, L47
Alonso-Herrero, A., et al. 2006, ApJ, 640, 167
Balogh, M. L., Couch, W. J., Smail, I., Bower, R. G., & Glazebrook, K. 2002, MNRAS, 335, 10
Barnes, J. E., & Hernquist, L. E. 1991, ApJ, 370, L65
Barnes, J. E., & Hernquist, L. 1996, ApJ, 471, 115
Barton, E. J., Arnold, J. A., Zentner, A. R., Bullock, J. S., & Wechsler, R. H. 2007, ApJ, 671, 1538
Barton, E. J., Geller, M. J., & Kenyon, S. J. 2000, ApJ, 530, 660
Baugh, C. M., Lacey, C. G., Frenk, C. S., Granato, G. L., Silva, L., Bressan, A., Benson, A. J., & Cole, S. 2005, MNRAS, 356, 1191
Beisbart, C., & Kerscher, M. 2000, ApJ, 545, 6
Bell, E. F., & de Jong, R. S. 2001, ApJ, 550, 212
Bell, E. F., McIntosh, D. H., Katz, N., & Weinberg, M. D. 2003, ApJS, 149, 289
Bell, E. F., et al. 2004, ApJ, 608, 752
Bell, E. F., et al. 2005, ApJ, 625, 23
Bell, E. F., et al. 2006, ApJ, 652, 270
Bell, E. F., et al. 2007, ApJ, 663, 834
Boerner, G., Mo, H., & Zhou, Y. 1989, A&A, 221, 191
Borch, A., et al. 2006, A&A, 453, 869
Brown, M. J. I., et al. 2007, ApJ, 654, 858
Caldwell, J., et al. 2008, ApJS, 174, 136
Chabrier, G. 2003, ApJ, 586, L133
Chapman, S. C., Smail, I., Windhorst, R., Muxlow, T., & Ivison, R. J. 2004, ApJ, 611, 732
Chary, R., & Elbaz, D. 2001, ApJ, 556, 562
Colless, M., et al. 2001, MNRAS, 328, 1039
Conselice, C., et al. 2003, AJ, 126, 1183
Cox, T. J. 2004, PhD thesis, Univ. California, Santa Cruz
Cox, T. J., Jonsson, P., Primack, J. R., & Somerville, R. S. 2006a, MNRAS, 373, 1013
Cox, T. J., Jonsson, P., Somerville, R. S., Primack, J. R., & Dekel, A. 2008, MNRAS, 384, 386
Cox, T. J., et al. 2006b, ApJ, 643, 692
Cox, T. J., et al. 2006c, ApJ, 650, 791
Davis, M., & Peebles, P. J. E. 1983, ApJ, 267, 465
De Lucia, G., et al. 2006, MNRAS, 366, 499
Devriendt, J. E. G., Guiderdoni, B., & Sadat, R. 1999, A&A, 350, 381
di Matteo, P., Bournaud, F., Martig, M., Combes, F., Melchior, A.-L., & Semelin, B. 2008, A&A, 492, 31
di Matteo, T., Springel, V., & Hernquist, L. 2005, Nature, 433, 604
di Matteo, P., et al. 2007, A&A, 468, 61
Emsellem, E., et al. 2004, MNRAS, 352, 721
Faber, S. M., et al. 2007, ApJ, 665, 265
Fioc, M., & Rocca-Volmerange, B. 1997, A&A, 326, 950
Fioc, M., & Rocca-Volmerange, B. 1999, arXiv:astro-ph/9912179
Ford, H., et al. 2003, Proc. SPIE, 4854, 81
Gray, M. E., et al. 2009, MNRAS, 393, 1275
Hammer, F., et al. 2005, A&A, 430, 115
Hernández-Toledo, H. M., Avila-Reese, V., Conselice, C. J., & Puerari, I. 2005, AJ, 129, 682
Hopkins, A. M. 2004, ApJ, 615, 209
Hopkins, P. F., Cox, T. J., Younger, J. D., & Hernquist, L. 2009, ApJ, 691, 1168
Jogee, S., et al. 2009, ApJ, 697, 1971
Jonsson, P., Cox, T. J., Primack, J. R., & Somerville, R. S. 2006, ApJ, 637, 255
Kartaltepe, J. S., et al. 2007, ApJS, 172, 320
Kaviraj, S., Peirani, S., Khochfar, S., Silk, J., & Kay, S. 2009, MNRAS, 394, 1713
Kroupa, P. 2001, MNRAS, 322, 231
Kroupa, P., Tout, C. A., & Gilmore, G. 1993, MNRAS, 262, 545
Lambas, D. G., et al. 2003, MNRAS, 346, 1189
Le Fèvre, O., et al. 2000, MNRAS, 311, 565
Le Floch, E., et al. 2005, ApJ, 632, L169
Lehmer, D., et al. 2008, ApJ, 681, 1163
Li, C., Kauffmann, G., Heckman, T. M., Jing, Y. P., & White, S. D. M. 2008, MNRAS, 385, 1903
Lilly, S. J., Le Fevre, O., Hammer, F., & Crampton, D. 1996, ApJ, 460, L1
Lin, L., et al. 2007, ApJ, 660, L51
Lisker, T. 2008, ApJS, 179, 319
Lotz, J., et al. 2004, AJ, 128, 163
Madau, P., et al. 1996, MNRAS, 283, 1388
Masjedi, M., et al. 2006, ApJ, 644, 54
Melbourne, J., Koo, D. C., & Le Floc'h, E. 2005, ApJ, 632, L65
Mihos, J. C., & Hernquist, L. 1994, ApJ, 431, L9
Mihos, J. C., & Hernquist, L. 1996, ApJ, 464, 641
Miller, S., et al. 2008, New Horizons in Astron., 393, 236
Noeske, K. G., et al. 2007, ApJ, 660, L43
Papovich, C., & Bell, E. F. 2002, ApJ, 579, L1
Papovich, C., et al. 2004, ApJS, 154, 70
Patton, D. R., et al. 2000, ApJ, 536, 153
Pérez-González, P. G., Trujillo, I., Barro, G., Gallego, J., Zamorano, J., & Conselice, C. J. 2008, ApJ, 687, 50
Ramos Almeida, C., Pérez García, A. M., Acosta-Pulido, J. A., & Rodríguez Espinosa, J. M. 2007, AJ, 134, 2006
Risaliti, G., Maiolino, R., & Salvati, M. 1999, ApJ, 522, 157
Rix, H.-W., et al. 2004, ApJS, 152, 163
Robertson, B., et al. 2006a, ApJ, 641, 21
Robertson, B., et al. 2006b, ApJ, 645, 986
Robertson, B., et al. 2006c, ApJ, 641, 90
Roussel, H., Sauvage, M., Vigroux, L., & Bosma, A. 2001, A&A, 372, 427
Sanders, D. B., et al. 1988, ApJ, 325, 74
Schweizer, F., & Seitzer, P. 1992, AJ, 104, 1039
Silva, L., Maiolino, R., & Granato, G. L. 2004, MNRAS, 355, 973
Skibba, R. A., & Sheth, R. K. 2009, MNRAS, 392, 1080
Skibba, R., et al. 2006, MNRAS, 369, 68

Somerville, R. S., Primack, J. R., & Faber, S. M. 2001, MNRAS, 320, 504
Somerville, R. S., et al. 2008, MNRAS, 391, 481
Spinoglio, L., Malkan, M. A., Rush, B., Carrasco, L., & Recillas-Cruz, E. 1995, ApJ, 453, 616
Springel, V. 2000, MNRAS, 312, 859
Tissera, P. B., Domínguez-Tenreiro, R., Scannapieco, C., & Sáiz, A. 2002, MNRAS, 333, 327
Toomre, A., & Toomre, J. 1972, ApJ, 178, 623
Trager, S. C., Faber, S. M., Worthey, G., & González, J. J. 2000, AJ, 119, 1645
Walcher, C. J., et al. 2008, A&A, 491, 713
Wolf, C., Meisenheimer, K., Rix, H.-W., Borch, A., Dye, S., & Kleinheinrich, M. 2003, A&A, 401, 73
Wolf, C., et al. 2004, A&A, 421, 913
Wolf, C., et al. 2005, ApJ, 630, 771
Zheng, X. Z., Bell, E. F., Papovich, C., Wolf, C., Meisenheimer, K., Rix, H.-W., Rieke, G. H., & Somerville, R. 2007a, ApJ, 661, L41
Zheng, X. Z., Dole, H., Bell, E. F., Le Floc'h, E., Rieke, G. H., Rix, H.-W., & Schiminovich, D. 2007b, ApJ, 670, 301